Light *p*-shell nuclei with cluster structures ($4 \leqslant A \leqslant 16$) in nuclear matter

Gerd Röpke
Institut für Physik, Universität Rostock, D-18051 Rostock, Germany
and National Research Nuclear University (MEPhI), 115409 Moscow, Russia

(Received 20 March 2020; accepted 21 May 2020; published 15 June 2020)

The composition of hot and dense nuclear matter is calculated including the $1p$-shell nuclei $4 \leqslant A \leqslant 16$. In-medium shifts, in particular Pauli blocking, are determined by the intrinsic wave function of the nuclei. Results are given within a shell-model approach for the nucleon wave function. Light nuclei are not always well described by the shell model. The "clustered" nucleus ^{8}Be exhibits strong correlation effects because of α-like clustering. Intrinsic cluster structures are also significant for the nuclei ^{6}Li, ^{7}Li, ^{7}Be, and ^{9}Be. The contribution of the relatively rare elements Li, Be, and B, to the equation of state (EoS) of matter near the saturation density is overestimated in simple approaches such as the nuclear statistical equilibrium (NSE) model. Both the treatment of continuum correlations and the account of in-medium modifications are considered for the contribution of ^{5}He and ^{4}H clusters. Compared to the extended NSE including unstable nuclei, the contributions of the corresponding $P_{3/2}$ channel with $A = 5, Z = 2$ and P_2 channel with $A = 4, Z = 1$, respectively, to the EoS are strongly suppressed at high densities owing to Pauli blocking effects. For the shifts of the binding energies of the light *p*-shell nuclei, simple-fit formula are given to calculate the composition of hot and dense matter in a wide parameter range.

DOI: 10.1103/PhysRevC.101.064310

I. INTRODUCTION

Nuclear systems, such as nuclei, excited matter produced in heavy-ion collisions, and nuclear matter found in compact astrophysical objects, are strongly coupled quantum systems. The traditional treatment [1] of dense nuclear systems which is based on a single-nucleon quasiparticle approach, such as the relativistic mean-field approximation, the shell model of nuclei, and the transport models related to the Boltzmann equation, has to be improved to describe quantum correlations, in particular the formation of bound states (clusters). Four-nucleon, α-like correlations have been considered to describe nuclei such as the Hoyle state of ^{12}C (see Refs. [2,3] and references given there), but are also of relevance to describe the α decay of heavy nuclei [4]. The production of clusters in heavy-ion collisions (HIC) (see, e.g., Refs. [5,6]), demands the treatment of clusters in highly excited nuclear matter which can be realized within a quantum statistical approach [7]. In thermodynamic equilibrium, in simplest approximation a mass action law is obtained describing chemical equilibrium in a mixture of ideal, noninteracting components performing reactive collisions, which is denoted as nuclear statistical equilibrium (NSE) [8]. Improvements are obtained by taking into account excited states, in particular the contribution of the continuum to obtain virial expansions [7,9,10]. In nonequilibrium, codes such as the antisymmetrized molecular dynamics (AMD) and quantum molecular dynamics (QMD) have been developed to include cluster formation in the treatment of HIC; see Ref. [11]. The equation of state of stellar matter in a wide range of temperature T, baryon density $n_B = n_n^{\rm tot} + n_p^{\rm tot}$, and asymmetry $Y_p = n_p^{\rm tot}/n_B$ is of interest in supernovae explosions (see Refs. [12,13] and references given there), and the account of few-nucleon correlations and cluster formation is relevant for the treatment of different processes during the evolution of compact astrophysical objects. As an alternative to the total number densities $n_\tau^{\rm tot}$ of neutrons ($\tau = n$) and protons ($\tau = p$), the state of nuclear matter can also be described by the chemical potentials μ_τ, in addition to T.

The simple NSE and its improvements considering excited states and scattering phase shifts of the isolated few-nucleon problem cannot be applied to baryon number densities near the saturation density $n_{\rm sat} = 0.15$ fm^{-3} where the interaction between the constituents cannot be neglected. A systematic quantum statistical approach to thermodynamic equilibrium can be given which uses the concepts of Green's functions, spectral functions, and frequency-dependent self-energy, for which a cluster decomposition can be performed. A main feature is that bound states can be treated as quasiparticles with medium-dependent binding energies and wave functions. They are obtained from an in-medium Schrödinger equation derived within a Green's function approach [7]. In addition to the single-nucleon self-energy, the antisymmetrization of the wave function (Pauli principle) is of relevance. Starting from the mass action law at low densities, clusters become less bound at increasing densities because of Pauli blocking. They are dissolved at a critical density so that near the saturation density a Fermi liquid model of single-nucleon quasiparticles becomes applicable. In particular, the contribution of two-nucleon correlation has been discussed at arbitrary densities [14]. The inclusion of light clusters $A \leqslant 4$, i.e. deuteron d (^{2}H), triton t (^{3}H), helion h (^{3}He), and α (^{4}He), has also been investigated; see Ref. [15] and references given there. Only

TABLE I. Data of (nearly) stable nuclei $A \leqslant 16$ as well as ^{5}He and ^{8}Be. Mass number A, charge number Z, binding energy per nucleon $B_{A,Z}/A$, and degeneracy factor $g = 2J + 1$ [22]. Solar element abundance: $\log_{10}$ relative to 12 for hydrogen; [square brackets] denote isotope fraction [32]. Half-life in seconds, days, years, and gigayears according to Ref. [22]. Charge rms radii taken from Ref. [33]. Parameter values $\bar{B}$ (13), the ansatz $B_s(A) = 1.324\,A^{-1/6}$ fm^{-1} as well as the parameter $\beta = B_s^2/B_p^2$ are also given.

A	Z	$\frac{B_{A,Z}}{A}$ [MeV]	$g_{A,Z}$	Abundance/half-life	$\mathrm{rms}_{\mathrm{charge}}$ [fm]	$\mathrm{rms}_{\mathrm{point}}$ [fm]	$\bar{B}$ [fm^{-1}]	B_s [fm^{-1}]	β
1	1		2	12 [0.99998]	0.8783	0			
2	1	1.112	3	12 [0.00002]	2.1421	1.9538	0.627		
3	1	2.827	2	12.32 y (β^-)	1.7591	1.5242	0.928		
3	2	2.572	2	10.93 [0.000166]	1.9661	1.7590	0.804		
4	2	7.073	1	10.93 [0.999834]	1.6755	1.427	1.051	1.051	
5	2	5.512	4	2.04×10^{-22} s					
6	3	5.332	3	1.05 [0.07594]	2.589	2.435	0.731	0.982	2.533
7	3	5.606	4	1.05 [0.9241]	2.444	2.281	0.812	0.957	1.626
7	4	5.372	4	53 d (ec)	2.646	2.496	0.742	0.957	2.065
8	4	7.062	1	8.19×10^{-17} s					
9	4	6.462	4	1.38 [1.0]	2.519	2.438	0.797	0.918	1.444
10	4	6.497	1	1.5 Gy (β^-)	2.355	2.185	0.904	0.902	0.995
11	4	5.953	2	13 s (β^-)	2.463	2.301	0.869	0.888	1.055
10	5	6.475	7	2.70 [0.199]	2.4277	2.263	0.873	0.902	1.089
11	5	6.928	4	2.70 [0.801]	2.4060	2.240	0.893	0.888	0.986
12	6	7.680	1	8.43 [0.98894]	2.4702	2.309	0.875	0.875	1.0
13	6	7.470	2	8.43 [0.01062]	2.4614	2.2994	0.886	0.864	0.939
14	6	7.520	1	5700 y (β^-)	2.5025	2.3433	0.876	0.853	0.938
14	7	7.476	1	7.83 [0.99771]	2.5582	2.4027	0.854	0.853	0.996
15	7	7.699	2	7.83 [0.00229]	2.6058	2.4533	0.842	0.843	1.003
16	8	7.976	1	8.69 [0.99762]	2.6991	2.5522	0.814	0.834	1.059

first steps have been made to include higher clusters $A > 4$ [16] within this approach.

The present work is devoted to the investigation of clusters with mass number $4 \leqslant A \leqslant 16$ where, in addition to the $1s$ shell, the $1p$ shell is filled. A list of the corresponding stable nuclei is given in Table I, together with some known properties. There are some recent works to include $1p$-shell nuclei in the calculation of the equation of state and the composition of hot and dense matter. In Ref. [17], unstable, neutron-rich isotopes such as ^{4}H, ^{5}He, and isotopes with even higher neutron content have been included in the NSE. A strong dominance of neutron-rich isotopes is found at high densities and low proton fraction Y_p. In-medium effects may be included within an excluded-volume approach [18] but the dominance of unstable, neutron-rich isotopes at high densities remains. Another approach to include $1p$ nuclei in the EoS [19] has been proposed within a generalized RMF approach [20], where all nuclei are considered as new quasiparticles and the corresponding fields are coupled to the meson fields. These semiempirical approaches should be founded by a more systematic quantum statistical approach as indicated in this work.

In this work, I focus on two aspects of the inclusion of light p-shell nuclei, the in-medium modification and dissolution of bound states at increasing density owing to Pauli blocking and the account of continuum correlation within a generalized cluster Beth-Uhlenbeck approach. Fit formulas are proposed to reproduce the energy shifts and the virial coefficients, i.e., the partial intrinsic partition functions, which are needed to calculate the composition of nuclear matter in a wide parameter range. These expressions can be used for the evaluation of the EoS but are also of interest for other applications such as kinetic and transport processes in subsaturation nuclear matter; see Ref. [11] and references given there.

The paper is organized as follows: After a short review of the formalism in Sec. II with the focus on Pauli blocking, the in-medium shifts of the binding energy of bound $1p$ nuclei are discussed in Sec. III. Because Pauli blocking is connected with the occupation in phase space, the wave function of the bound states in momentum representation is essential and will be discussed in Sec. III A. To discuss the contribution of unstable nuclei such as ^{4}H and ^{5}He, it is necessary to consider the continuum correlations in Sec. IV. Illustrative calculations for the composition of nuclear systems are presented and discussed in Sec. V. One finds that in comparison to the NSE, the mass fraction of $1p$ nuclei is significantly reduced near the saturation density if in-medium effects are systematically taken into account.

II. BASIC EXPRESSIONS

A. Composition of dense nuclear matter

Within a strict quantum statistical approach [15], nuclear matter in thermodynamic equilibrium is characterized by the temperature T and the chemical potentials μ_τ. Neglecting weak processes, there are two conserved quantities, the total number of neutrons and protons (bound in nuclei and free ones) with the corresponding chemical potentials μ_n, μ_p. As an equation of state, the total densities n_τ^{tot} of neutrons and

protons are obtained using the method of thermodynamic Green's functions via the single-nucleon spectral functions or the related self-energy. At subsaturation baryon densities $n_B = n_n^{\rm tot} + n_p^{\rm tot} \leqslant n_{\rm sat}$, I am interested in cluster formation which is described by the cluster decomposition of the self-energy. As a result, the total densities of neutrons and protons are given as the sum of free nucleons and the nucleons bound in clusters,

$$\begin{aligned} n_n^{\rm tot}(T,\mu_n,\mu_p) &= \frac{1}{\Omega}\sum_{A,Z,J,\nu,\mathbf{P}} N f_{A,Z}(E_{A,Z,J,\nu}(\mathbf{P};T,\mu_n,\mu_p)) \\ &= \sum_{A,Z,J} N n_{A,Z,J}^{\rm part}(T,\mu_n,\mu_p), \\ n_p^{\rm tot}(T,\mu_n,\mu_p) &= \frac{1}{\Omega}\sum_{A,Z,J,\nu,\mathbf{P}} Z f_{A,Z}(E_{A,Z,J,\nu}(\mathbf{P};T,\mu_n,\mu_p)) \\ &= \sum_{A,Z,J} Z n_{A,Z,J}^{\rm part}(T,\mu_n,\mu_p)\,, \end{aligned} \tag{1}$$

i.e., the sum over the partial densities of the different channels characterized by $\{A,Z,J\}$. $N = A - Z$ is the neutron number, Ω is the volume, and $\mathbf{P}$ denotes the center of mass (c.m.) momentum of the cluster (or, for $A = 1$, the momentum of the nucleon). The internal quantum state ν describes possible intrinsic excitations of the A-nucleon cluster, and

$$f_{A,Z}(\omega;T,\mu_n,\mu_p) = \frac{1}{\exp[(\omega - N\mu_n - Z\mu_p)/T] - (-1)^A} \tag{2}$$

is the Bose or Fermi distribution function for even or odd A, respectively. For parameter values considered here, the free nucleons may become degenerate. For all other clusters, the classical approximation is possible at $T > 1$ MeV.

In the low-density, low-temperature limit, one can take the ground-state energies (the negative of the binding energies)

$$E_{A,Z,J,\nu}(\mathbf{P};T,\mu_n,\mu_p) \approx E_{A,Z,J}^{(0)} + \hbar^2 P^2/(2Am) \tag{3}$$

and perform the summation over $\mathbf{P}$ and ν (degeneracy factor $2J+1$) so that the partial density of channel $\{A,Z,J\}$ results as

$$n_{A,Z,J}^{\rm part,0}(T,\mu_n,\mu_p) = (2J+1)\left(\frac{AmT}{2\pi\hbar^2}\right)^{3/2} e^{(-E_{A,Z,J}^{(0)} + N\mu_n + Z\mu_p)/T}. \tag{4}$$

Here, m denotes the nucleon mass (the proton-neutron mass difference is neglected). The bound state energies $E_{A,Z,J}^{(0)} = -B_{A,Z}$ and the degeneracy $2J+1$ are found in the tables of nuclei [21,22]. This approximation for the EoS is also denoted as nuclear statistical equilibrium (NSE). It describes an ideal mixture of nuclei (bound states), interacting only occasionally via reactive collisions.

The simple approximation (4) can be improved in different ways. First, not only the ground state $E_{A,Z,J}^{(0)}$ but also the excited states ν of the nucleus with quantum numbers $\{A,Z,J\}$ contribute to the partial densities (4). In particular, the scattering states describing continuum correlations have to be taken into account. If the scattering states of two clusters are described by the scattering phase shifts $\delta_{A,Z,J}(E)$ with $\nu \to E$ as the energy of relative motion, the virial EoS is derived from a quantum statistical approach [7,9,10,14,23,24]. This contribution of scattering states as given by the Beth-Uhlenbeck equation is discussed in Sec. IV.

Second, with increasing density, the approximation of noninteracting clusters is no longer possible, and medium modifications have to be considered. A quantum statistical approach can be used; see Ref. [15] and further references given there. In particular, a quasiparticle approach can be given where the energies of the nucleons and of the nuclei, $E_{A,Z,J,\nu}(\mathbf{P};T,\mu_n,\mu_p)$, are depending on the temperature and baryon densities of the nuclear medium. In addition, the dependence on the c.m. momentum $\mathbf{P}$ is more general than the expression (3). These modifications are given by the self-energy of the single-nucleon states and the Pauli blocking on the interaction within the clusters; for details, see Ref. [15] for $A \leqslant 4$. Also the bound-state wave functions and the scattering phase shifts are modified. These medium modifications for the bound states with $4 \leqslant A \leqslant 16$ are discussed in Sec. III.

B. In-medium shift of bound nuclei

In the low-density limit, the virial form of the EoS can be calculated knowing the empirical values of the cluster binding energies and the scattering phase shifts. The knowledge of the interaction potential is not necessary. This is not the case at higher densities where the medium modifications have to be taken into account. Within the quantum statistical approach, one has to solve the A-particle in-medium Schrödinger equation (momentum representation)

$$\begin{aligned} &\left[E_{\tau_1}^{\rm qu}(1) + \cdots + E_{\tau_A}^{\rm qu}(A) - E_{A,Z,J,\nu}(\mathbf{P};T,\mu_n,\mu_p)\right] \\ &\quad\times \Psi_{A\nu P}(1\ldots A) + \sum_{1'\ldots A'}\sum_{i<j}\left[1 - f_{\tau_i}(i) - f_{\tau_j}(j)\right] \\ &\quad\times V(ij,i'j')\prod_{k\neq i,j}\delta_{kk'}\Psi_{A\nu P}(1'\ldots A') = 0, \end{aligned} \tag{5}$$

where $1 = \{\mathbf{p}_1,\sigma_1,\tau_1\}$ denotes momentum, spin, and isospin variables. $E_{\tau_1}^{\rm qu}(1)$ are quasiparticle energies which are obtained from a frequency-dependent self-energy. Parametrizations for the quasiparticle energies [20] can be used which are derived from relativistic mean-field approximations such as the density-dependent relativistic mean-field (DD2-RMF) approximation [25] or an effective mass approximation. The self-energy shift acts for the bound states as well as for the continuum and has no influence on the binding energy in the rigid shift approximation where the $\mathbf{p}$ dependence of the shift is neglected. Then, it can be implemented in the chemical potential. Within the effective mass approximation, a minor effect on the shift of the binding energy was obtained in Ref. [26].

More important is the Pauli blocking given by the occupation number $f_{\tau_i}(i)$ of the single-nucleon state i in front of the interaction potential in Eq. (5). Neglecting the correlations in the surrounding medium, one can use a Fermi distribution function with effective values for temperature and chemical potential to approximate the actual occupation numbers. Single-nucleon states which are already occupied cannot be used to build up the bound state wave function $\Psi_{A\nu P}(1\ldots A)$.

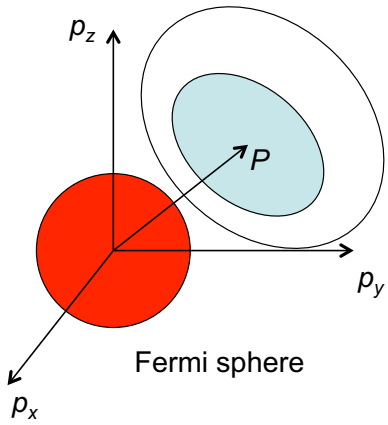

FIG. 1. Pauli blocking: In momentum space $\{p_x, p_y, p_z\}$, the Fermi sphere is occupied. A bound state is formed around the c.m. momentum $\mathbf{P}$ using free phase space. Contributions of the occupied Fermi sphere cannot be used to form the bound-state wave function.

As a consequence, the binding energy $-E_{A,Z,J,\nu}(\mathbf{P};T,\mu_n,\mu_p)$ is shifted, depending on the cluster intrinsic quantum numbers ν and the c.m. momentum $\mathbf{P}$, but also on temperature T and chemical potentials μ_τ. A schematic representation of the Pauli blocking and its dependence on the c.m. momentum $\mathbf{P}$ is shown in Fig. 1.

For the light clusters $A \leqslant 4$, the Pauli blocking has been discussed in the literature [15,26,27]. An effective separable potential $V(ij,i'j')$ has been considered which reproduces known properties, in particular the binding energies and rms radii. Similar calculations to determine the in-medium energy shifts as function of temperature, densities of protons and neutrons, and the c.m. momentum can also be performed for larger, weakly bound clusters; see Appendix A.

For large numbers A, an appropriate description of the nucleon wave function is the shell model where the A-nucleon wave function is approximated by the antisymmetrized product (Slater determinant) of single-nucleon wave functions obtained from an effective potential $V^{\rm mf}(1,1')$. A widely used local potential is the Woods-Saxon potential [28]. Bound and scattering states are easily obtained from a separable potential [29,30], which will also be used here; see Appendix B. Note that any local potential can be expressed as sum of separable potentials [31].

Within the shell model, the nucleons are moving independently on single-particle orbits. Instead of Eq. (5), one has to solve the single-nucleon wave equations

$$E^{\rm qu}_{\tau_1}(1)\,\psi_{1\nu P}(1) + \sum_{1'}\big[1-f_{\tau_1}(1)\big]\,V^{\rm mf}(1,1')\,\psi_{1\nu P}(1') = E^{\rm qu}_{1\nu}(\mathbf{P};T,\mu_n,\mu_p)\,\psi_{1\nu P}(1), \tag{6}$$

where the dependence of the c.m. momentum $\mathbf{P}$ results from the relative motion of the Fermi distribution $f_{\tau_1}(1)$. The Pauli blocking shift of the single-nucleon states follows as

$$\Delta E^{\rm Pauli}_{1\nu}(\mathbf{P};T,\mu_n,\mu_p) = \sum_{11'}\psi_{1\nu P}(1)\,f_{\tau_1}(1)\,V^{\rm mf}(1,1')\psi_{1\nu P}(1'). \tag{7}$$

An important ingredient to calculate in-medium effects is the nucleon wave function of the A-nucleon cluster. In the simplest form of a density functional approach, the Thomas-Fermi model, the many-particle wave function is approximated locally by plane waves, and shell effects are not described. The shell model starts from the approximation of the antisymmetrized product of single-nucleon quasiparticle orbits and has to include correlation effects. Alternative concepts to approximate the many-nucleon wave function are based on the cluster model which adequately includes, for instance, α-like clustering in light nuclei, in particular ^{8}Be or the Hoyle state of ^{12}C; see Refs. [2,3] and Sec. III C below.

III. PAULI BLOCKING OF p-SHELL NUCLEI

A. Intrinsic nucleon wave function of a cluster

To calculate the in-medium shifts, the intrinsic wave function of the nucleons in the nucleus (cluster) is needed. I focus here on the Pauli blocking which is responsible for the disappearance of bound states with increasing density. As seen from Fig. 1, this effect is determined by the wave function in momentum space and the overlap with the Fermi distribution function. Therefore, in this section I intend to find appropriate approximations for the intrinsic wave function. The self-energy corrections cancel nearly with the shift of the continuum and give only a small contribution to the in-medium shift of the binding energy which describes the energy difference, but must be included in the bound-state energy $E_{A,Z,J,\nu}$; see Ref. [26] and Sec. V.

One can try to extract the wave function from empirical data, in particular the rms radii; cf. Ref. [27] for the light $1s$ nuclei $A \leqslant 4$. In Sec. III B, I consider the nuclear shell model. The $1p$ nuclei with $5 \leqslant A \leqslant 16$ are described by the successive occupation of the $1p$ orbit. Independent mean-field orbitals are considered, while correlations and spin-orbit interaction are neglected. To treat strong correlations in the nucleon wave function, the formation of subclusters is discussed in Sec. III C.

I use Gaussian wave functions, which have the advantage that the center-of-mass (c.m.) motion can be separated from the intrinsic motion. The Gaussian wave function has been considered in Ref. [26] for the light nuclei and compared to a Jastrow function approach. The differences of the results for the Pauli blocking shift are small so that it can be concluded that details of the wave function are not very important; only the global distribution in phase space and the overlap with the Fermi sphere are relevant.

The shell-model wave functions of interest are the $1s$ and $1p$ states with different width parameters B_s, B_p, respectively,

$$\psi_{1s}(\mathbf{r}) \propto e^{-r^2B_s^2/4}\,Y_{00}(\theta,\phi),$$
$$\psi_{1p}(\mathbf{r}) \propto e^{-r^2B_p^2/4}\,r\,Y_{1m}(\theta,\phi), \tag{8}$$

or, in Fourier space,

$$\psi_{1s}(\mathbf{p}) \propto e^{-p^2/B_s^2}\,Y_{00}(\theta,\phi),$$
$$\psi_{1p}(\mathbf{p}) \propto e^{-p^2/B_p^2}\,p\,Y_{1m}(\theta,\phi). \tag{9}$$

The ratio of the squared width parameters will be denoted by $\beta = B_s^2/B_p^2$. The A-nucleon wave function

$$\Psi_{A,\nu}(1,\ldots,A) = \mathcal{A}\{\psi_{1s,\nu_1}(1)\ldots\psi_{1s,\nu_4}(4) \times \psi_{1p,\nu_5}(5)\ldots\psi_{1p,\nu_A}(A)\} \quad (10)$$

is approximated by the antisymmetrized product (Slater determinant) of occupied orbitals, ν denotes the quantum numbers of the cluster, and the intrinsic quantum number ν_i contains spin and isospin of the single nucleon.

The point rms radius of the A-nucleon cluster follows as square root of

$$\langle r^2\rangle_{A,\nu} = \frac{1}{A}\langle\Psi_{A,\nu}|\sum_i^A(\mathbf{r}_i - \mathbf{R}_{\rm cm})^2|\Psi_{A,\nu}\rangle, \quad (11)$$

with the c.m. position $\mathbf{R}_{\rm cm} = A^{-1}\sum_i^A \mathbf{r}_i$. For $A \leqslant 4$, the nucleons occupy $1s$ orbits. After introduction of Jacobi coordinates, the c.m. part can be separated, and the intrinsic part gives [26]

$$\langle r^2\rangle_{A,\nu} = \frac{3(A-1)}{A\,B_s^2}, \quad A \leqslant 4. \quad (12)$$

The same result is obtained if taking $\mathbf{R}_{\rm cm} = 0$ so that $\mathbf{r}_1 = -\mathbf{r}_2 - \cdots - \mathbf{r}_A$.

For larger nuclei $4 \leqslant A \leqslant 16$, the $1p$ orbitals are successively occupied. Assuming $\beta = 1$, i.e., assuming $B_s = B_p$ and denoting this common value as $\bar{B}$, one obtains for the point rms radii the square root of

$$\langle r^2\rangle_{A,\nu} = \frac{3(A-1)+2(A-4)}{A\,\bar{B}^2}, \quad 4 \leqslant A \leqslant 16, \quad (13)$$

which can be used to derive this common parameter $\bar{B}$ from the observed rms radii.

For $\beta = B_s^2/B_p^2 \neq 1$, the expressions for the rms radii are more complex. As example, for $A = 6$ one finds (A3)

$$\langle r^2\rangle_{^6{\rm Li}} = \frac{\beta}{6B_s^2}\frac{21 + 160/\beta + 382/\beta^2 + 688/\beta^3 + 288/\beta^4}{(1+2/\beta)(3+8/\beta+16/\beta^2)}. \quad (14)$$

For $4 \leqslant A \leqslant 16$ and arbitrary β, as approximation to results like Eq. (14) I assume the sum of a contribution from the $1s$ orbit (four nucleons) and a contribution from the $1p$ orbit [$(A-4)$ nucleons],

$$\langle r^2\rangle_{A,\nu} \approx \frac{9}{A\,B_s^2} + \frac{5A-20}{A\,B_p^2}, \quad 4 \leqslant A \leqslant 16. \quad (15)$$

The nucleon wave functions should reproduce the measured rms radii shown in Table I. This is essential for the correct determination of the distribution in momentum space and the calculation of Pauli blocking.

In Table I, the stable nuclei with mass number $A \leqslant 16$ are shown, together with nuclei with half-life larger than 1 s. For comparison, the nucleus ^{5}He and the interesting nucleus ^{8}Be are also included. The binding energy per nucleon $B_{A,Z}/A$ [22] and degeneracy are given. Note that the binding energy per nucleon for ^{8}Be is quite large compared to the neighboring nuclei. However, it is not stable as shown by the very short half-life. It decays into two α particles, which have even higher values for the binding energy per nucleon. There is also no stable nucleus with the mass number $A = 5$. Within the shell-model approach, the nucleon added to the ^{4}He core has to be positioned in the $1p$ state at higher kinetic energy so that binding does not occur. ^{5}He-like correlations are discussed below in Sec. IV B. All other nuclei have a binding energy larger than the sum of the binding energies of respective cluster components.

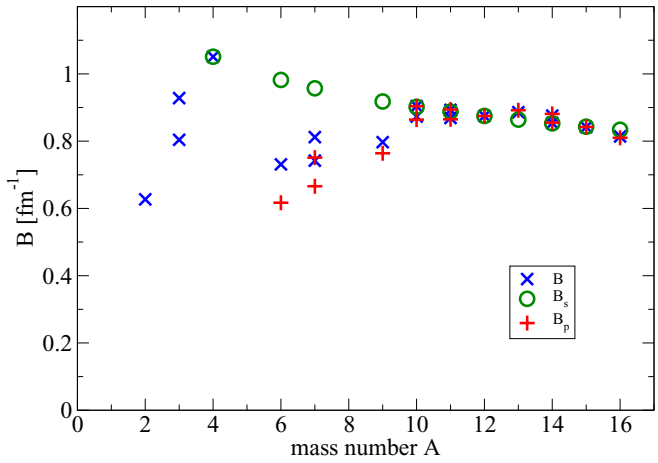

FIG. 2. The range parameter B of the Gaussian orbits. $\bar{B}$ according to (13) (blue crosses) as well as B_s (green circles) and B_p (red plus) as function of the mass number A.

The unstable, long-living isotopes given in Table I have weak interaction decays (electron capture for ^{7}Be, β^- for ^{3}H, ^{10}Be, and ^{11}Be). For the stable nuclei, the solar element abundances are given, in addition to the isotope fractions [32]. Compared to the elements C, N, and O, the clustered "rare" elements Li, Be, and B have very low abundance. Note that missing bound nuclei with $A = 5, 8$ are relevant for nucleosynthesis in astrophysics.

In Table I, values for the charge rms radii and point rms radii, $\text{rms}^2_{\rm point} = \text{rms}^2_{\rm charge} - 0.8783^2\,\text{fm}^2$, are taken from Ref. [33]. The rms radii do not exhibit a simple dependence on A as expected, e.g., for a liquid drop model. Details of the A-nucleon wave function are of relevance. The nuclear shell model describes already important properties of the A-nucleon wave function. Correlations which also influence the rms radii, in particular clustering [2], are discussed below in Sec. III C.

The deuteron is weakly bound and therefore extended in configuration space. The difference of the rms radii of t and h is well understood; see Ref. [27], Appendix A. The α particle is a compact, strongly bound nucleus. The wave functions of these light nuclei are reasonably described by a Gaussian $1s$ wave function [26]. The calculation of $\bar{B}$ according to Eq. (13) assuming $\beta = 1$ is shown in Table I; see also Fig. 2. A smooth behavior is obtained for $A \geqslant 10$. The clustered nuclei with $6 \leqslant A \leqslant 9$ demand a further discussion of the nucleon wave function.

In the general systematics (see Ref. [33]), the rms value for ^{6}Li is relatively large. Within the nuclear shell-model approach, two nucleons are positioned in the $1p$ state weakly

TABLE II. Potential parameter $V_{0,s}^{\rm WS}, V_{0,p}^{\rm WS}$ and Pauli blocking shift $\Delta E_{A,Z}^{\rm Pauli}(P=0;T,n_B,Y_p) \approx n_B\, \delta E_{A,Z}^{\rm Pauli}(T)$, approximated by two interpolation fits. First version: $\delta E_{A,Z}^{\rm Pauli}(T) \approx A\, a_{AZ}\, \exp(-b_{AZ}T)$. Second version: $\delta E_{A,Z}^{\rm Pauli}(T) \approx A\, f_{AZ}/(T+g_{AZ})^{3/2}$. Units: MeV, fm.

A	Z	B_s [fm^{-1}]	$V_{0,s}^{\rm WS}$ [MeV]	B_p [fm^{-1}]	$V_{0,p}^{\rm WS}$ [MeV]	a_{AZ} [MeV fm^3]	b_{AZ} [MeV^{-1}]	f_{AZ} [MeV$^{5/2}$ fm^3]	g_{AZ} [MeV]
4	2	1.051	73.7			796.1	0.06002	50621	14.291
6	3	0.982	63.8	0.617	35.2	640.6	0.06427	35278	12.771
7	3	0.957	60.8	0.751	41.6	599.9	0.06188	35845	13.624
7	4	0.957	60.8	0.666	35.2	598.4	0.06440	32834	12.737
9	4	0.918	56.8	0.764	40.5	549.3	0.06094	33943	13.990
10	4	0.902	55.3	0.904	61.0	541.5	0.05148	47499	18.281
11	4	0.888	54.3	0.865	54.1	532.4	0.05290	46823	18.482
10	5	0.902	55.3	0.864	53.8	539.4	0.05414	42678	16.916
11	5	0.888	54.3	0.894	59.7	534.8	0.05068	48450	18.730
12	6	0.875	53.3	0.875	56.6	529.1	0.05085	47663	18.653
13	6	0.864	52.7	0.892	60.9	531.7	0.04821	53382	20.217
14	6	0.853	52.0	0.881	59.5	531.9	0.04801	53891	20.358
14	7	0.853	52.0	0.855	54.0	526.8	0.05039	48385	18.929
15	7	0.843	51.6	0.842	52.2	528.1	0.05071	47916	18.763
16	8	0.834	51.2	0.810	46.9	524.2	0.05297	43513	17.555

bound to the α-like core. One can account for weakly bound, more extended nucleons in the $1p$ state if one constructs the shell-model wave function (10) with different parameter values B_s, B_p, i.e., with $\beta \neq 1$. Strong deviations are expected for the clustered nuclei ^{6}Li, ^{7}Li, ^{7}Be, and ^{9}Be, whereas the nuclei with $A \geqslant 10$ behave smoothly.

For an exploratory calculation within a shell-model approach, I assume that the inner $1s$ wave function changes smoothly if A is increasing. With the ansatz $B_s(A) = 1.324\, A^{-1/6}$ fm^{-1} the values $\bar{B}$, Table I, are approximately reproduced for $A \geqslant 10$. Then, the parameter values B_p given in Table I follow from Eq. (15). For $A = 6$, the value $B_s(6) = 0.982$ fm^{-1} is estimated. To reproduce the empirical value of the point rms radius of ^{6}Li, with Eq. (14) one finds $\beta = 2.533$, i.e., $B_p = 0.617$ fm^{-1}. These values are also confirmed by a more detailed six-nucleon calculation given below in Appendix A.

The results shown in Table I and Fig. 2 describe only properties of the wave function as derived from the rms radii. The α-like core changes smoothly, but the outer $1p$ nucleons show a particular behavior for $5 \leqslant A \leqslant 9$. Small values of B_p means that the $1p$ orbital is very extended. As a consequence, the density is low, and correlation effects become relevant. A signature is cluster formation which appears in the low-density regions, as known from the Hoyle state. Here, the many-nucleon wave function has another structure. For ^{8}Be, it is described in good approximation by the Tohsaki-Horuichi-Schuck-Röpke (THSR) wave function [2]. Clustering in nuclei [34–36] will be discussed below in Sec. III C.

B. Shell-model approach

For large numbers A, an appropriate description of the nucleon wave function is the shell model where the single-nucleon wave functions are obtained from an effective potential. Within local potentials, a well-known example is the Woods-Saxon potential

$$V^{\rm mf,WS}(r) = V_0^{\rm WS}/[1 + e^{(r-R_A)/a}]. \tag{16}$$

Typical parameter values which reproduce the properties of heavy nuclei are $V_0^{\rm WS} = 52.06$ MeV, $R_A = 1.26A^{1/3}$ fm, and $a = 0.662$ fm [28]. However, the light nuclei are not well described by these fit parameters.

To calculate Pauli blocking, one needs the effective potential to reproduce the nucleon wave functions. I take the general form (16) with parameters which reproduce the rms values. Within a variational approach, I consider the Gaussians as class of wave functions and find the parameter values of (16) for which the solutions of the wave function reproduce the values of B_s and $B_p = B_s\beta^{-1/2}$ presented in Table I. From the three parameters $V_0^{\rm WS}$, R_A, and a, occurring in Eq. (16), I fix $R_A = 1.26A^{1/3}$ fm and $a = 0.662$ fm as given above. Thus, I consider $V_0^{\rm WS}$ as a fit parameter to reproduce the rms values of the corresponding nucleon wave functions. The solutions $V_{0,s}^{\rm WS}, V_{0,p}^{\rm WS}$ are given for the $A \leqslant 16$ nuclei in Table II. The values $V_{0,s}^{\rm WS}$ are consistent with the value $V_0^{\rm WS}$ [28] for the larger nuclei. The values $B_s(A), B_p(A)$ are also shown in in Fig. 2. The decrease of B_s for increasing A is given by the ansatz $B_s(A) = 1.324\, A^{-1/6}$ fm^{-1} given above and describes the smooth change of the α-like $1s$ core with increasing A. The values of B_p show strong deviations from B_s for small $A < 10$. This may be considered as a signature that the wave function of these exotic nuclei is not well described by the shell model as discussed in Sec. III C.

With the potential, one can calculate the Pauli blocking shift of the cluster as the sum over the shift (7) of the single-nucleon states. Approximating the Fermi distribution by the classical distribution

$$f_\tau(1) \approx \frac{n_\tau}{2}\left(\frac{2\pi\hbar^2}{mT}\right)^{3/2} e^{-\hbar^2 p_1^2/(2mT)} \tag{17}$$

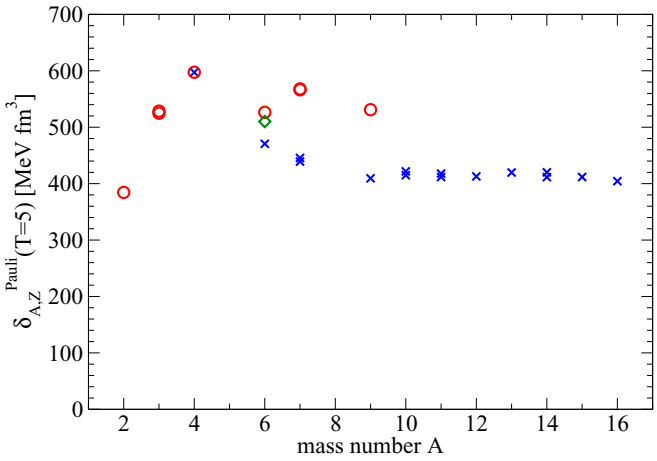

FIG. 3. Pauli-blocking shift $\delta E^{\rm Pauli}_{AZ}(T)$ of $1s$, $1p$ nuclei ($A \leqslant 16$) at $T = 5$ MeV. Shell-model calculations (blue crosses) are compared to cluster model calculations (red circles). The green diamond gives the result of a microscopic calculation for ^{6}Li. Values for $A < 4$ are taken from Ref. [26].

valid in the low-density region ($\mu_\tau < 0$), a linear dependence on the baryon density results. In general, one has

$$\begin{aligned}\Delta E^{\rm Pauli}_{A,Z}(P;T,\mu_n,\mu_p) &= \sum_\nu \Delta E^{\rm Pauli}_{1,\nu} \\ &= n_B F_{A,Z}(Y_p)\,\delta E^{\rm Pauli}_{A,Z}(P;T) + \mathcal{O}\big(n_B^2\big). \end{aligned} \tag{18}$$

For symmetric matter ($n_n = n_p$) follows $F_{A,Z}(Y_p) = 1$, and for asymmetric matter one has

$$n_B\, F_{A,Z}(Y_p) = \frac{2}{A}(N n_n + Z n_p). \tag{19}$$

Results are presented here for $P = 0$. For the light $1s$ elements, the **P** dependence is discussed in Ref. [15]. According to Eqs. (7) and (18), one has $\delta E^{\rm Pauli}_{A,Z}(T) = 4\,\delta E^{\rm Pauli}_{AZ,s}(T) + (A-4)\,\delta E^{\rm Pauli}_{AZ,p}(T)$. The separate contributions of the four nucleons in the s orbit and the $(A-4)$ nucleons in the p orbit are given in Appendix C, Table VIII, for different T; see also Fig. 3. Interpolations for $\delta E^{\rm Pauli}_{A,Z}(T)$ are shown in Table II; see Sec. III D below.

A consequence of the Pauli blocking is that the in-medium binding energy of the cluster is decreasing with increasing density. In Ref. [7], the Mott density $n^{\rm Mott}_{A,Z}(T) = B_{A,Z}/\delta E^{\rm Pauli}_{A,Z}(P=0,T)$ has been introduced, characterizing the density where the bound state is dissolved. It depends on T as shown in Table VIII of Appendix C. In general, the Mott condition $B_{A,Z} - \Delta E^{\rm Pauli}_{A,Z}(P;T,\mu_n,\mu_p) = 0$ gives a critical baryon density which depends not only on T but also on **P** and asymmetry. In the case of ^{6}Li, one has the situation where the bound state dissolves into a (medium-modified) α particle and two nucleons. This leads to further reduction of the Mott density.

Note that the values for the Mott density given in Table VIII in Appendix C cannot be interpreted such that any A-nucleon correlations disappear for increasing density at this value. Above the Mott density, bound states may exist for $\mathbf{P} \neq 0$ where the blocking is smaller; see the decreasing overlap with increasing $|\mathbf{P}|$ in Fig. 1. In addition, correlations are present in the continuum (see Sec. IV B below) and contribute to the composition of nuclear matter above the Mott density [14].

C. Cluster model

The main issue to calculating the Pauli blocking is the knowledge of the many-nucleon wave function, which determines the phase space occupation. The shell model is based on the concept of independent motion in a mean-field potential. As a quasiparticle approach, correlations between the nucleons are neglected. However, this model is problematic for nuclei with small mass numbers.

The "clustered" elements Li, Be, and B are weakly bound p-shell nuclei which demand special treatment. Whereas the ground states of C, N, and O ($12 \leqslant A \leqslant 16$) may be reasonably approximated by a shell model, it fails for the lighter nuclei because of the strong clustering contribution to the ground-state wave function. Clustering in nuclei is treated by the resonating group method (RGM) and related approaches; see Refs. [37–40] and references given there.

A striking example is ^{8}Be. In contrast to other light $n\alpha$ nuclei which are stable and have relative large binding energy, ^{8}Be ($n = 2$) is unstable and decays in two α particles; see Table I. The reason is the strong quartet clustering, and *ab initio* calculations [41] show a dumbbell-shaped intrinsic density distribution. Similar to the Hoyle state which also clearly shows a cluster structure, the THSR approach [2] has been worked out to describe α-like clustering in nuclei. Significant cluster structures are also observed in the neighboring nuclei ^{7}Li, ^{7}Be, and ^{9}Be using AMD (antisymmetrized molecular dynamics) calculations [36]. For recent inelastic scattering, see Ref. [42]. Whereas ^{9}Be can be discussed as a two-α bound state hold together by the additional neutron, ^{7}Li and ^{7}Be can be considered as bound states of $\alpha + {}^3$H and ^{3}He, respectively. Also, ^{6}Li may be contain deuteron-like correlations in addition to the α particle. The density distribution of the intrinsic ground state of ^{9}Be is shown in Ref. [34].

The wave function of the cluster model is given by the antisymmetrized product of the wave functions of the constituent subclusters. For instance, the THSR approach considers ^{8}Be as antisymmetrized product of two α-like Gaussians with two different width parameters describing the intrinsic motion and the center-of-mass motion of the constituent subclusters. The intrinsic density distribution of these clustered nuclei is characterized by two α-like cluster for ^{8}Be and ^{9}Be. The Pauli blocking shift results mainly from the blocking of the intrinsic motion of these subclusters, so I approximate this by the sum of the Pauli blocking of the constituents. Considering ^{7}Be, ^{7}Li, and ^{6}Li in the same way, I calculate the Pauli blocking shifts as the sum of the shifts of the constituent subclusters. The shifts of the corresponding light clusters are given in Ref. [26] (denoted by asterisks). Using the expression (46) of Ref. [26] to calculate the Pauli blocking shifts of the constituents, one finds

$$\Delta E^{\rm Pauli}_{A,Z}(P;n_B,Y_p,T) \approx n_B\, F_{A,Z}(Y_p)\, A\, \frac{f_{A,Z}}{(T+g_{A,Z})^{3/2}}, \tag{20}$$

TABLE III. Cluster states: A^* (the asterisk denotes that information about the shifts is taken from Ref. [26]). Ac denotes the adapted α shift from shell-model calculation. Pauli blocking shift $\Delta E^{\rm Pauli}_{A,Z}(P=0;T,n_B,Y_p) \approx n_B\,\delta E^{\rm Pauli}_{A,Z}(T)$ is approximated by two interpolation fits. First version: $\delta E^{\rm Pauli}_{A,Z}(T) \approx A\,a_{AZ}\,\exp(-b_{AZ}T)$. Second version: $\delta E^{\rm Pauli}_{A,Z}(T) \approx A\,f_{AZ}/(T+g_{AZ})^{3/2}$. Units: MeV, fm.

A	Z	$\delta E^{\rm Pauli}_{A,Z}(5)/A$ [MeV fm^3]	$\delta E^{\rm Pauli}_{A,Z}(20)/A$ [MeV fm^3]	a_{AZ} [MeV fm^3]	b_{AZ} [MeV^{-1}]	f_{AZ} [MeV$^{5/2}$ fm^3]	g_{AZ} [MeV]
2*	1	384.4	79.0	695.6	0.12216	8715.8	3.011
3*	1	524.8	160.8	791.1	0.08550	23175	7.493
3*	2	528.5	146.3	831.5	0.09412	19482	6.0765
4*	2	662.5	241.9	931.3	0.07117	41092	10.670
4	2	597.3	252.1	796.1	0.06002	50621	14.291
6*	3	569.8	187.6	834.7	0.07997	28374	8.545
6c	3	526.5	194.4	737.5	0.07096	32603	10.673
7*	3	603.5	207.1	869.1	0.0762	32990	9.406
7c	3	566.3	212.9	787.5	0.06908	37030	11.237
7*	4	605.0	200.9	882.9	0.07897	30926	8.776
7c	4	567.9	206.7	799.6	0.07178	34554	10.480
9*	4	588.8	215.0	827.9	0.07117	36527	10.670
9c	4	531.0	224.0	707.7	0.06002	44996	14.291

with $F_{A,Z}(Y_p)$ given by Eq. (19). As before, I take $P=0$, neglecting the $\mathbf{P}$ dependence of the Pauli shift. Values for the parameter $f_{A,Z}$ and $g_{A,Z}$ are given in Table III. The Gaussian approach for the wave functions is used, but for consistency the shift of the α particle is taken according to the present shell-model approach, Table II, which slightly differs because the c.m. motion is not separated. These cluster values are denoted by c. They are used in the further discussion. Results are also shown in Fig. 3.

In Appendix A, the cluster model approximation described here is checked by considering the lightest clustered nucleus ^{6}Li. A microscopic calculation is performed using an effective nucleon-nucleon interaction potential and separating of the c.m. motion. A large value of the Pauli blocking is obtained; see Table V in Appendix B. Note that the Pauli blocking is stronger for the cluster structure than the shell-model value. The wave function in the $1s$ state is large at $p=0$, but goes to zero for the $1p$ state so that the overlap with the Fermi distribution becomes small.

D. Interpolation formula

Let us consider the contribution to the energy shift, Eq. (18), which is linear in the baryon density. A calculation of the full density dependence of the energy shift has been performed for the deuteron [14], which shows that the contribution of correlations to the density is strongly suppressed above the Mott density. For the light elements, an expression for the contribution $\propto n_B^2$ has been given in Ref. [15]. As example, the quadratic term $\propto n_B^2$ for the energy shift of ^{5}He is calculated below in Eq. (42). I suppose that the linear term of the energy shift is sufficient to describe the Mott effect. The higher order terms of the density expansion may become relevant near the saturation density. They need a special treatment that is in general beyond the scope of the present work. One can expect that near the saturation density any correlations beyond the quasiparticle approach are fading away. A detailed description of this behavior is available at present only for some special cases such as ^{2}H and ^{5}He [14].

Calculations for the Pauli blocking shift $\delta E^{\rm Pauli}_{A,Z}(T)$ have been performed for all p-shell nuclei for $1\,{\rm MeV} \leqslant T \leqslant 20$ MeV and baryon densities up to the Mott density; see, e.g., Table VIII in Appendix C. To implement the in-medium shifts in calculations of the composition of nuclear matter and related properties, I propose interpolation expressions for the Pauli blocking shift

$$\Delta E^{\rm Pauli}_{A,Z}(P;T,n_B,Y_p) \approx n_B\,F_{A,Z}(Y_p)\,A\;a_{A,Z}\;e^{-b_{A,Z}T}, \qquad (21)$$

where the dependence on $\mathbf{P}$ is neglected, thus taking $P=0$. With the results shown in Table VIII in Appendix C, one obtains from a least square deviation fit the values $a_{A,Z}$ and $b_{A,Z}$ given in Tables II and III; see also Fig. 4. The relative deviations of the interpolation fit (21) are less than 2% in the region considered here.

A similar fit (20) has been proposed in Ref. [26] for the light cluster $A \leqslant 4$. The values $f_{A,Z}$ and $g_{A,Z}$ are also given in Tables II and III. The relative deviations are less than 4%. Within the parameter region discussed here, both interpolation formulas give similar results. However, outside this region, (20) overestimates the behavior at low temperatures where the phase space near $\mathbf{p}=0$ is relevant. There, the $1p$ wave function has zero density so that Pauli blocking is less efficient. This lower value for the Pauli blocking is better reproduced by expression (21).

Within this work, I use the fit (21). The Pauli blocking shifts $\Delta E^{\rm Pauli}_{A,Z}$ are nearly proportional to the mass number A. The corresponding parameter values $a_{A,Z}$ and $5000 b_{A,Z}$ are shown in Fig. 4. For the nuclei $10 \leqslant A \leqslant 16$, one has the average values $\bar{a} = 532.0\,{\rm MeV\,fm^3}$ and $\bar{b} = 0.05103\,{\rm MeV^{-1}}$. These values are also shown in Fig. 4 (dotted lines). In conclusion, the expression

$$\Delta E^{\rm Pauli}_{A,Z}(P;T,\mu_n,\mu_p) \approx A F_{A,Z}(Y_p) 532.0\, e^{-0.05103\,T/[{\rm MeV}]} n_B[{\rm MeV\,fm^3}] \qquad (22)$$

works for $1p$ nuclei with $10 \leqslant A \leqslant 16$.

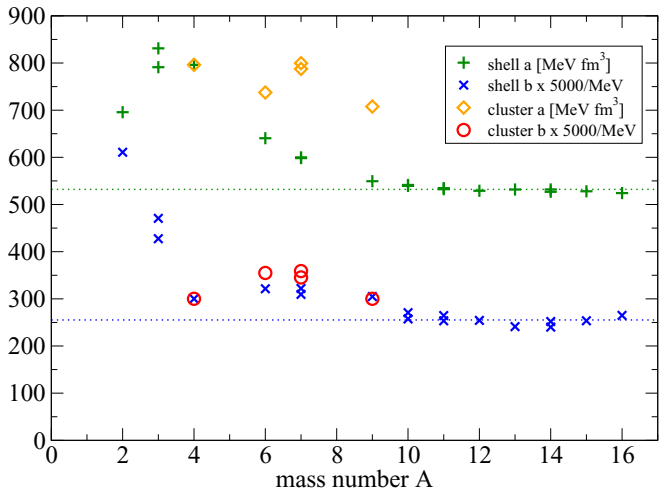

FIG. 4. Parameter values of the fit (21). The values $a_{A,Z}$ [MeV fm^3] and $5000 b_{A,Z}$ [MeV^{-1}] are shown. Dotted lines are the averages $\bar{a} = 532.0$ MeV fm^3 and $\bar{b} = 0.05103$ MeV^{-1}. Shell-model calculations are denoted by green plus signs ($a_{A,Z}$) and blue crosses ($b_{A,Z}$); cluster model calculations are shown by orange diamonds ($a_{A,Z}$) and red circles ($b_{A,Z}$).

For the lighter, clustered nuclei, the shell-model approach considering a wave function formed by $1s, 1p$ orbitals is not applicable. The strong deviation of $a_{A,Z}$, $b_{A,Z}$ from the average values $\bar{a}$, $\bar{b}$, respectively, are caused by the anomalous large rms radii of the rare element nuclei and clustering effects.

IV. EQUATION OF STATE INCLUDING SCATTERING STATES AND LOOSELY BOUND OBJECTS

A. Generalized Beth-Uhlenbeck approach

The equation of state (1) includes the sum over excited states ν, in particular, the continuum of scattering states. Considering $1p$ nuclei, excited states are of relevance. As an example, the contribution of the channel describing few-nucleon correlations with $A = 8$ to the equation of state contains also the nucleus ^{8}Be. Sometimes it is included in NSE as a real nucleus, decaying quickly into two α particles.

A more systematic quantum statistical approach is necessary to treat continuum correlations. In the S-wave $\alpha + \alpha$ channel, ^{8}Be appears as a resonance and contributes to the virial coefficient b_α investigated in Ref. [10]. Similarly, unstable nuclei in other channels should be treated as continuum correlations via the scattering phase shifts. The need to treat scattering states is evident when considering in-medium effects and the dissolution of bound states because of Pauli blocking. The bound-state contribution to the partial densities (1) shows a discontinuous behavior if a bound state merges with the continuum and disappears. This discontinuity is compensated for taking into account continuum contributions according to the Levinson theorem.

To describe these effects, the intrinsic partition function $z^{\rm part}_{A,Z,J}(\mathbf{P}; T, \mu_n, \mu_p)$ of the channel $\{A, Z, J\}$ at $\mathbf{P}$ is introduced in Ref. [15],

$$n^{\rm part}_{A,Z,J}(T, \mu_n, \mu_p) = \int \frac{d^3P}{(2\pi)^3} e^{-\hbar^2 P^2/(2AmT)} e^{(N\mu_n + Z\mu_p)/T} z^{\rm part}_{A,Z,J}(\mathbf{P}; T, \mu_n, \mu_p). \tag{23}$$

A further subdivision into a bound part and a continuum part, $z^{\rm part}_{A,Z,J}(\mathbf{P}; T, \mu_n, \mu_p) = z^{\rm bound}_{A,Z,J}(\mathbf{P}; T, \mu_n, \mu_p) + z^{\rm cont}_{A,Z,J}(\mathbf{P}; T, \mu_n, \mu_p)$, is not free of ambiguity. One can choose as bound-state contribution

$$z^{\rm bound}_{A,Z,J}(\mathbf{P}; T, \mu_n, \mu_p) = (2J+1) e^{-E^{\rm cont}_{A,Z,J}(\mathbf{P})/T} \sum_\nu^{\rm bound} [e^{B_{A,Z,J,\nu}(\mathbf{P};T,\mu_n,\mu_p)/T} - 1] \Theta[B_{A,Z,J,\nu}(\mathbf{P}; T, \mu_n, \mu_p)], \tag{24}$$

where the in-medium binding energy is given by $B_{A,Z,J,\nu}(\mathbf{P}) = -E_{A,Z,J,\nu}(\mathbf{P}) + E^{\rm cont}_{A,Z,J}(\mathbf{P})$. Here, $E^{\rm cont}_{A,Z,J}(\mathbf{P})$ is the edge of continuum in the channel under consideration. The quasiparticle approach is used where the density effects are taken into account in the mean-field approximation. In particular, the single-nucleon states are shifted by the self-energy. As example, one can use the parametrization [15,20] of the relativistic mean-field approximation DD2-RMF [25]. For the bound-state energies $E_{A,Z,J,\nu}(\mathbf{P}; T, \mu_n, \mu_p)$, I take the solution of the in-medium Schrödinger equation (5) containing the single-particle shifts and the Pauli blocking (21); see Ref. [26]. The -1 in the bound-state contribution (24) is a relict of the scattering state contribution according to the Levinson theorem; see Eq. (26) below. It makes the bound-state contribution continuous if the binding energy goes to zero. Here, the continuum edge of the cluster constituents at the same total momentum $\mathbf{P}$ is for the decay into single nucleons

$$E^{\rm cont}_{A,Z,J}(\mathbf{P}; T, \mu_n, \mu_p) = N E_n(\mathbf{P}/A; T, \mu_n, \mu_p) + Z E_p(\mathbf{P}/A; T, \mu_n, \mu_p). \tag{25}$$

A similar relations gives the edge of the continuum if other decay channels containing subclusters are considered. The argument of the step function $\Theta(x) = 1, x \geqslant 0$; $= 0$ else, denotes the binding energy which must be positive to have a bound state. Above the Mott density, this condition is a restriction for the summation over $\mathbf{P}$ to that region where bound states may exist. If the quasiparticle shift is taken in effective mass approximation, the shift can be transferred to the chemical potential.

The contribution of two interacting clusters to the EoS is related to the scattering phase shifts according to Beth and Uhlenbeck [9,43]. For instance, for the deuteron channel $^2\mathrm{H} = d$ ($A = 2, Z = 1, J = 1$) one has the generalized Beth-Uhlenbeck formula [14]

$$z^{\rm part}_d(\mathbf{P}; T, \mu_n, \mu_p) = e^{-\frac{\hbar^2 P^2}{4mT} - \frac{E^{\rm cont}_d(P)}{T}} 3 \Big[\big(e^{B_d(P)/T} - 1\big) \Theta[B_d(P)] + \frac{1}{\pi T} \int_0^\infty dE\, e^{-E/T} \Big\{ \delta_d(E) - \frac{1}{2} \sin[2\delta_d(E)] \Big\} \Big] \tag{26}$$

with medium-modified bound-state energies and phase shifts also obtained from the in-medium Schrödinger equation (5) to be consistent. The generalized Beth-Uhlenbeck formula [14] considers already the quasiparticle distribution so that the single-particle energies are shifted by a mean-field contribution. Note that the term $-\frac{1}{2}\sin[2\delta_d(E)]$ in Eq. (26) compensates the contributions already used for the mean-field shift of the single-nucleon quasiparticle energies [14]. Thus, double counting of interaction terms is avoided.

In the low-density limit, the in-medium modifications can be neglected, and the Fermi and/or Bose distributions are replaced by the Boltzmann distribution. In this ordinary Beth-Uhlenbeck formula for the second virial coefficient, the single-particle contribution is described by the distribution of free, noninteracting nucleons. The integral over $\mathbf{P}$ in Eq. (26) can be performed and

$$n_d^{\mathrm{part},0}(T) = 3\left(\frac{2mT}{2\pi\hbar^2}\right)^{3/2} e^{(\mu_n+\mu_p)/T}\left[e^{-E_d^{(0)}/T} - 1 + \frac{1}{\pi T}\int_0^\infty dE\; e^{-E/T}\delta_d^{(0)}(E)\right] \tag{27}$$

results.

The scattering phase shift $\delta_d^{(0)}(E)$ as function of the kinetic energy E of relative motion is mainly given by $\delta_{^3\mathrm{S}_1}(E)$; for a more detailed discussion of the low-density limit, see Ref. [10]. There, the full contribution to the spin-triplet channel contains also the phase shifts $\delta_{^3\mathrm{D}_1}(E)$, etc. Within the virial expansion, one has

$$n_d^{\mathrm{part},0}(T) = 4/\Lambda^3 e^{(\mu_n+\mu_p)/T} b_d^0(T), \tag{28}$$

where $\Lambda^2 = 2\pi\hbar^2/(mT)$ and

$$b_d^0(T) = \frac{3}{\sqrt{2}}\left[e^{-E_d^{(0)}/T} - 1 + \frac{1}{2\pi T}\int_0^\infty dE_{\mathrm{lab}} \times e^{-E_{\mathrm{lab}}/2T}\delta_d^{(0)}(E_{\mathrm{lab}})\right], \tag{29}$$

if the single nucleon contribution is given by the free nucleons, $n_\tau^{\mathrm{part},0}(T) = 2\Lambda^{-3}e^{\mu_\tau/T}$. Here, E_{lab} is the energy of the projectile hitting the resting target. Continuum contributions to the cluster-second virial coefficient from nucleon-nucleon, nucleon-α, and α-α scattering phase shifts have been given in Ref. [10].

The inclusion of scattering phase shifts between two components of the cluster $\{A, Z, J\}$ is seen from the square brackets in Eqs. (26), (27), and (29) and suggests defining the intrinsic channel partition function

$$C_{A,Z,J}(P) = \sum_\nu^{\mathrm{bound}} (e^{B_{A,Z,J,\nu}(P)/T} - 1)\Theta[B_{A,Z,J,\nu}(P)] + \frac{1}{\pi T}\int_0^\infty dE\; e^{-E/T}\left\{\delta_{A,Z,J}(E,P) - \frac{1}{2}\sin[2\delta_{A,Z,J}(E,P)]\right\} \tag{30}$$

where E is the c.m. energy. The integral part in Eq. (30) describing the continuum contribution was denoted in Ref. [15] as residual second virial coefficient. Binding energies and scattering phase shifts contain in-medium corrections so that they depend, in general, on $\mathbf{P}, T, \mu_n, \mu_p$. Calculating this expression, the artificial subdivision in bound and continuum contributions becomes obsolete. A generalized phase shift may be introduced containing contributions of negative E, where at each bound-state energy a jump of π happens; see Ref. [15].

In-medium corrections are treated within the generalized Beth-Uhlenbeck approach [14] for the nucleon-nucleon system. In this work, the treatment of light clusters [15,26,27] is extended to the $1p$ nuclei. One has to determine the medium modifications of the scattering phase shifts solving Eq. (5). This in-medium Schrödinger equation contains a potential, and, as usual, one can choose the potential to reproduce the free scattering phase shifts. I will use a separable potential which leads to simpler expressions for the Pauli blocking; see Appendix B.

B. ^{5}He, no in-medium shifts

For equilibrium nuclear matter with low proton fraction Y_p, neutron-rich nuclei are dominant. In particular, triton t (^{3}H) is more abundant than helion h (^{3}He). Also, the neutron-rich nuclei ^{4}H, ^{5}He, ^{6}He, etc., may become relevant [17]. However, they are not stable. One has to consider the channels, for which they appear as resonances in the continuum of scattering states.

In this subsection, I focus on ^{5}He. It belongs to the channel with $A = 5, Z = 2, J = 3/2$ which contains the contribution of the unstable nucleus. The binding energy $B_{^5\mathrm{He}} = 27.56$ MeV [22] is smaller than the binding energy of ^{4}He so that $\Delta B_{^5\mathrm{He},\alpha n} = B_{^5\mathrm{He}} - 28.3\,\mathrm{MeV} = -0.7356$ MeV. It decays as $^5\mathrm{He} \to \alpha + n$; the half-life is 7×10^{-22} s.

The partial density of the ^{5}He channel is (I consider the virial coefficient $b_{\alpha n}(T)$ for the $\alpha - n$ system [10])

$$n_{^5\mathrm{He}} = 16\left(\frac{mT}{2\pi\hbar^2}\right)^{3/2} b_{\alpha n}(T)\, e^{(-E_\alpha+3\mu_n+2\mu_p)/T}. \tag{31}$$

Within NSE, the partial density of this unstable nucleus would be (degeneracy $2J + 1 = 4$)

$$n_{^5\mathrm{He}}^{\mathrm{NSE}} = 4\left(\frac{5mT}{2\pi\hbar^2}\right)^{3/2} e^{(3\mu_n+2\mu_p+B_{^5\mathrm{He}})/T} = \frac{n_n}{2}n_\alpha 4\left(\frac{5}{4}\frac{2\pi\hbar^2}{mT}\right)^{3/2} e^{-0.7356\,\mathrm{MeV}/T} = 4n_\alpha\left(\frac{5}{4}\right)^{3/2} e^{\mu_n/T} e^{\Delta B_{^5\mathrm{He},\alpha n}/T}. \tag{32}$$

This partial density contributes to the total neutron density with the factor 3 and to the total proton density with the factor 2. For a bound state with bound-state energy $E_{^5\mathrm{He}} = -B_{^5\mathrm{He}} = -27.56$ MeV, one finds for relation (31)

$$b_{\alpha n}^{\mathrm{NSE}}(T) = \frac{5^{3/2}}{4} e^{(-E_{^5\mathrm{He}}+E_\alpha)/T}. \tag{33}$$

TABLE IV. $N-\alpha$ virial coefficient $b_{\alpha n}$, Eq. (34). The results of Ref. [10] using empirical phase shifts are compared to the NSE expression (33) and the Beth-Uhlenbeck calculations with phase shifts from two model potentials, a square well potential (sq. w.), and a separable potential (s. p.), considering only the contribution of the $P_{3/2}$ channel.

T [MeV]	$b_{\alpha n}^{\rm NSE}$	$b_{\alpha n}$ [10] full	$b_{\alpha n}$ [10] $P_{3/2}$ wave	$b_{\alpha n}^{\rm BU}$, sq. w. $P_{3/2}$ wave	$b_{\alpha n}^{\rm BU}$ s. p. $P_{3/2}$ wave
1	2.68	1.51	1.73	1.73	1.75
2	3.87	2.26	2.48	2.48	2.49
3	4.37	2.57	2.78	2.77	2.78
4	4.65	2.73	2.91	2.88	2.90
5	4.83	2.81	2.97	2.92	2.95
6	4.95	2.86	2.99	2.92	2.96
7	5.03	2.89	2.99	2.90	2.94
8	5.10	2.92	2.98	2.87	2.91
9	5.15	2.93	2.96	2.82	2.87
10	5.19	2.95	2.93	2.77	2.82
12	5.26	2.97		2.65	2.71
14	5.30	2.98		2.53	2.59
16	5.34	3.00		2.41	2.48
18	5.37	3.00		2.30	2.37
20	5.39	3.00		2.19	2.26

However, instead of the unstable nucleus, one has to treat the continuum contributions, in particular the phase shifts. It is an advantage of the Beth-Uhlenbeck formula that the second virial coefficient can be expressed in terms of properties which are directly observed, avoiding the introduction of a potential. As given in Ref. [10],

$$b_{\alpha n}^{\rm BU}(T) = \frac{5^{1/2}}{\pi T}\int_0^\infty dE_{\rm lab}\, e^{-4E_{\rm lab}/5T}\,\delta_{\alpha n}^{\rm tot}(E_{\rm lab}). \tag{34}$$

The relative energy is $(4/5)\,E_{\rm lab}$, the latter is the energy of the neutron, and the α is fixed. Scattering phase shifts for the different $\alpha-n$ channels are given in Ref. [44] and parametrized in Ref. [45], in particular (units: MeV):

$$\delta_{\rm P_{3/2}}(E_{\rm lab}) = \arccot\big[\big(0.1281 - 0.1095\,E_{\rm lab} + 0.006794\,E_{\rm lab}^2 - 0.000113\,E_{\rm lab}^3\big)\big/\big(0.043733\,E_{\rm lab}^{3/2}\big)\big] \tag{35}$$

which gives the main contribution to $\delta_{\alpha n}^{\rm tot}(E) = 2\delta_{\rm S_{1/2}} + 2\delta_{\rm P_{1/2}} + 4\delta_{\rm P_{3/2}} + \cdots$. Results for the virial coefficient (34), calculated with $\delta_{\alpha n}^{\rm tot}(E)$ as well as the main contribution $4\delta_{\rm P_{3/2}}$ at different values of T are shown in Table IV; see Ref. [10]. There exist also correlations in the other channels $(\delta_{\rm S_{1/2}}, \delta_{\rm P_{1/2}})$ which partially compensate each other, and higher angular momenta give almost no contribution to the density.

For comparison, calculations of phase shifts with a square well potential $V(r) = -V_0\Theta(a-r)$; $V_0 = 55$ MeV, $a = 2$ fm, as well as the separable potential given in Appendix B, Eq. (B1), with $\lambda = 670$ MeV fm^3, $\gamma = 1.791$ fm^{-1} are also given in Table IV. Both potentials are quite different but reproduce nearly the same phase shifts in the parameter region under consideration. The corresponding virial coefficients coincide in good approximation.

There is a significant contribution of the $P_{3/2}$ channel which allows us to introduce a nuclear state at negative binding energy $\Delta B_{^5{\rm He},\alpha n}^{\rm eff}(T)$. However, the NSE value $\Delta B_{^5{\rm He},\alpha n} = -0.736$ MeV overestimates the contribution of the ^{5}He channel. In particular, at high temperatures, the virial form gives lower values for the partial density, which is also known from the deuteron case. There, the introduction of an effective energy to account for the contribution of the continuum was also proposed in Ref. [24]. If comparing this generalized virial approach to the NSE, the contribution of the ^{5}He channel is essentially reduced, in particular at higher T.

C. ^{5}He, with in-medium shifts

As shown in Eq. (1), a cluster decomposition of the single-particle self-energy allows the decomposition of the total baryon density into partial densities. For $A > 1$, one obtains the contribution of the channel $\mathcal{C} = \{A, Z, J\}$

$$n_{A,Z,J}^{\rm part}(T,\mu_n,\mu_p) = (2J+1)\left(\frac{AmT}{2\pi\hbar^2}\right)^{3/2} e^{(-E_{A,Z,J}^{\rm cont}+N\mu_n+Z\mu_p)/T} \times C_{A,Z,J}(T,\mu_n,\mu_p), \tag{36}$$

neglecting quantum degeneracy and the $\mathbf{P}$ dependence of $C_{A,Z,J}(\mathbf{P};T,\mu_n,\mu_p)$ (30) so that the integral over the c.m. momentum $\mathbf{P}$ can be performed. Within a quasiparticle approach, in-medium bound-state energies and scattering phase shifts are used to evaluate the intrinsic channel partition function $C_{A,Z,J}$. Note that in general the $\mathbf{P}$ dependence may be taken into account within an effective mass approximation. The continuum edge $E_{A,Z,J}^{\rm cont}(\mathbf{P};T,\mu_n,\mu_p)$ (25) is also taken for $P = 0$. A binary effective interaction of subclusters $\mathcal{C}_1, \mathcal{C}_2$, with $\mathcal{C} \rightleftharpoons \mathcal{C}_1 + \mathcal{C}_2$, is considered which leads to the scattering phase shifts $\delta_{\mathcal{C};\mathcal{C}_1\mathcal{C}_2}(E)$, where E denotes the intrinsic energy of relative motion of the subclusters. The continuum edge $E_{\mathcal{C};\mathcal{C}_1,\mathcal{C}_2}^{\rm cont}(T,\mu_n,\mu_p) = E_{\mathcal{C}_1}^{\rm qu}(T,\mu_n,\mu_p) + E_{\mathcal{C}_2}^{\rm qu}(T,\mu_n,\mu_p)$ is obtained in the rigid shift approximation. I neglect the in-medium modification of the effective masses. As discussed above, the binding energy in the special binary channel $\Delta B_{\mathcal{C};\mathcal{C}_1\mathcal{C}_2}(T,\mu_n,\mu_p) = B_{\mathcal{C}} - E_{\mathcal{C};\mathcal{C}_1\mathcal{C}_2}^{\rm cont}$ relative to the corresponding continuum edge of subclusters has to be taken. The single-nucleon contribution ($A = 1$) follows from the quasiparticle shift calculated, e.g., from the DD2-RMF approach [20]. In general, the fermionic distribution function is used to calculate the single-nucleon densities.

Applying Eq. (36) to the binary reaction channel $\alpha + n \rightleftharpoons {}^5$He, $A = 5$, $Z = 2$, $J = 3/2$, one finds

$$n_{^5{\rm He}}^{\rm part}(T,\mu_n,\mu_p) = 4\left(\frac{5}{4}\right)^{3/2} n_\alpha(T,\mu_n,\mu_p) e^{-\Delta E_n^{\rm SE}/T+\mu_n/T} \times C_{^5{\rm He};\alpha n}(T,\mu_n,\mu_p), \tag{37}$$

with (there are no bound states)

$$C_{^5{\rm He};\alpha n}(T,\mu_n,\mu_p) = \frac{1}{\pi T}\int_0^\infty dE\, e^{-E/T}\left\{\delta_{^5{\rm He};\alpha n}(E) - \frac{1}{2}\sin[2\delta_{^5{\rm He};\alpha n}(E)]\right\} = \exp\big[-E_{^5{\rm He};\alpha n}^{\rm eff}(T,\mu_n,\mu_p)/T\big] \tag{38}$$

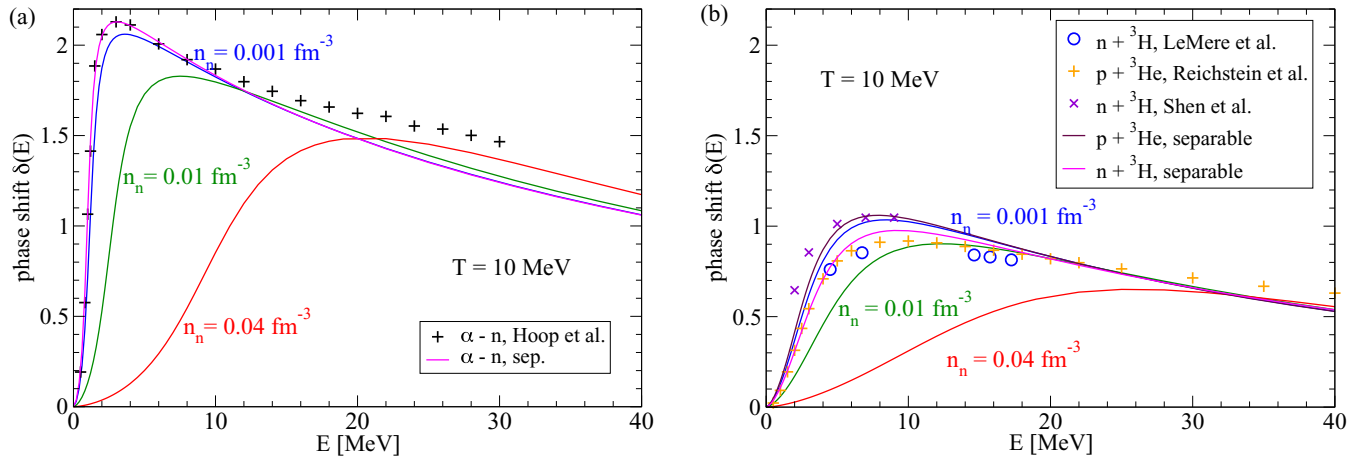

FIG. 5. In-medium scattering phase shifts for $\alpha - n$ (a) and $n - {}^3\mathrm{H}$, $p - {}^3\mathrm{He}$ (b). Experimental data of Hoop *et al.* [44] and Reichstein *et al.* [49] and calculations of LeMere *et al.* [47] and Shen *et al.* [48] are compared to the separable potentials with parameters given in the text. Medium modifications are shown for $T = 10$ MeV and different free neutron densities n_n.

with E being the energy of relative motion. For the sake of parametrization, I introduce the effective channel energy $E^{\rm eff}_{^5\mathrm{He};\alpha n}(T, \mu_n, \mu_p)$, which may be considered as an effective, medium-dependent excitation energy to describe the statistical weight of the corresponding channel. The in-medium scattering phase shifts contain the Pauli blocking effects, and single-nucleon self-energies cancel with continuum contributions in the rigid shift approximation.

Compared to (34), a more general Beth-Uhlenbeck (BU) result is [14]

$$b^{\rm gBU}_{\alpha n}(T, \mu_n, \mu_p) = 4\frac{5^{1/2}}{\pi T}\int_0^\infty dE_{\rm lab}\, e^{-4E_{\rm lab}/5T} \times \left\{\delta_{\alpha n}(E_{\rm lab}) - \frac{1}{2}\sin[2\delta_{\alpha n}(E_{\rm lab})]\right\} \quad (39)$$

with in-medium phase shifts; see Fig. 5. The free neutron density is calculated from the Fermi distribution function containing the quasiparticle shift $\Delta E^{\rm SE}_n$ (as before, the P dependence is neglected).

The values of $b_{\alpha n}(T, n_n)$ are calculated as function of the temperature T and the free neutron density n_n (only the motion of the neutron $1p$ orbit is blocked), using the BU formula [see (27)] and the generalized BU expression (39) [see (26)]. The partial density related to the channel $A = 5, Z = 2, J = 3/2$ is

$$n_{^5\mathrm{He}}(T, \mu_n, \mu_p) = \frac{8}{\Lambda^3} b_{\alpha n}(T, n_n)\, e^{[-E_\alpha(T,\mu_n,\mu_p)+2\mu_n+2\mu_p]/T} \times e^{(-\Delta E^{\rm SE}_n+\mu_n)/T}. \quad (40)$$

The free neutron density n_n is obtained from the Fermi distribution function with given T, μ_n, $\Delta E^{\rm SE}_n$. In-medium shifts for the α particle are taken from Ref. [26], and for the neutron shift $\Delta E^{\rm SE}_n$ one can use the parametrization [15] of the DD2-RMF approximation [25]. The calculations using a separable potential are given in Appendix B.

We scan the region $1 \leqslant T \leqslant 20$ MeV and $n_n \leqslant 0.1$ fm^{-3}. The results are parametrized as follows (note that the account of continuum contributions by effective energies has also been considered in Ref. [24]):

$$b_{\alpha n}(T, n_n) = \frac{5^{3/2}}{2} C_{^5\mathrm{He};\alpha n}(T, \mu_n, \mu_p) = \frac{5^{3/2}}{2} e^{-E^{\rm eff}_{\alpha n}(T,n_n)/T}. \quad (41)$$

For practical use, the dependence of the effective energy on the baryon density is approximated as

$$E^{\rm eff}_{\alpha n}(T, n_n) = E_{\alpha n,0}(T) + E_{\alpha n,1}(T)\, n_n + E_{\alpha n,2}(T)\, n_n^2. \quad (42)$$

Data presented in Table VI are reproduced with relative accuracy below 5% by the parameter values (units: MeV, fm)

$$\begin{aligned} E_{\alpha n,0}(T) &= 0.85503 + 0.21729\, T + 0.031362\, T^2; \\ E_{\alpha n,1}(T) &= 100.05 + 80.749 \ln T \\ &\quad + 384.08 \exp(-0.44383\, T); \\ E_{\alpha n,2}(T) &= -322.53 + 450.2 \ln T. \end{aligned} \quad (43)$$

D. ^{4}H

Of interest is the ^{4}H cluster in neutron-rich stellar matter. It belongs to the channel $A = 4, Z = 1, J = 2$. Similar to ^{5}He, it is not bound, and appears as correlations in the continuum of the $^3\mathrm{H} + n$ channel. Measured phase shifts for $^3\mathrm{H} + n$ are given in Ref. [46]; see also Refs. [47,48]. Of interest are the ${}^3\delta_1(E)$ phases as function of the c.m. energies E which are reproduced approximately by a separable potential ($B1$) with $\lambda = 1144.9$ MeV fm^3 and $\gamma = 1.326$ fm^{-1}.

The mirror cluster ^{4}Li appears in the $^3\mathrm{He} + p$ channel and is more extensively studied; see Ref. [49]. The corresponding virial coefficients have been considered in Ref. [50]; see also Ref. [51]. Here, the ${}^3\delta_1(E)$ phases as function of the c.m. energies E are reproduced approximately by a separable potential with $\lambda = 967.9$ MeV fm^3, $\gamma = 1.377$ fm^{-1}; see Fig. 5. As in the case of the mirror nuclei ^{3}H and ^{3}He, the potential is weaker as in the case $^3\mathrm{H} + n$ because of Coulomb repulsion.

I calculate according to Appendix B that

$$C_{^4\mathrm{H};tn}(P=0,T,\mu_n,\mu_p) = \frac{1}{\pi T}\int_0^\infty dE e^{-E/T}\left\{\delta_{^4\mathrm{H};tn}(E;P=0,T,\mu_n,\mu_p) - \frac{1}{2}\sin[2\delta_{^4\mathrm{H};tn}(E;P=0,T,\mu_n,\mu_p)]\right\}. \quad (44)$$

For parametrization, the effective energy $E^{\mathrm{eff}}_{tn}(P=0, T,\mu_n,\mu_p) = -T\ln[C_{^4\mathrm{H};tn}(P=0,T,\mu_n,\mu_p)]$ is introduced; see Table VII. The data in the Table VII are reproduced with relative accuracy of less than 2% by the approximation

$$E^{\mathrm{eff}}_{tn}(T,n_n) = E_{tn,0}(T) + E_{tn,1}(T)n_n \quad (45)$$

(higher order terms in n_n can be neglected), where the parameter values are (units: MeV, fm)

$$E_{tn,0}(T) = 3.0014 + 1.69165\,T + 0.025471\,T^2;$$
$$E_{tn,1}(T) = 334.62 + 97.424\ln T + 356.09\exp(-0.91636\,T). \quad (46)$$

For the partial density of ^{4}H one finds

$$n^{\mathrm{part}}_{^4\mathrm{H}}(T,\mu_n,\mu_p) = \frac{5}{2}\left(\frac{4}{3}\right)^{3/2} n_t(T,\mu_n,\mu_p) \times e^{-\Delta E^{\mathrm{SE}}_n/T+\mu_n/T} C_{^4\mathrm{H};tn}(T,\mu_n,\mu_p). \quad (47)$$

There is another channel $A=4, Z=1, J=1$ of ^{4}H containing the excited state $^4\mathrm{H}^*$ at 0.31 MeV excitation energy. In the present approach, to consider the scattering phase shifts one has to consider the $^1\delta_1(E)$ phases and finds the contribution

$$n^{\mathrm{part}}_{^4\mathrm{H}^*}(T,\mu_n,\mu_p) = \frac{3}{2}\left(\frac{4}{3}\right)^{3/2} n_t(T,\mu_n,\mu_p) \times e^{-\Delta E^{\mathrm{SE}}_n/T+\mu_n/T} C_{^4\mathrm{H}^*;tn}(T,\mu_n,\mu_p). \quad (48)$$

with the corresponding phase shifts, describing the known values [49]. Because the differences are small, one can assume that both contributions to the partial density can be put together. As before, I parametrize the result for the intrinsic channel partition function for both contributions as

$$n^{\mathrm{part}}_{^4\mathrm{H}}(T,\mu_n,\mu_p) \approx 4\left(\frac{4}{3}\right)^{3/2} n_t(T,\mu_n,\mu_p) \times e^{-\Delta E^{\mathrm{SE}}_n/T+\mu_n/T} C_{^4\mathrm{H};tn}(T,\mu_n,\mu_p), \quad (49)$$

$$C_{^4\mathrm{H};tn}(T,\mu_n,\mu_p) = \exp\left[E^{\mathrm{eff}}_{^4\mathrm{H};tn}(T,\mu_n,\mu_p)/T\right]. \quad (50)$$

There are also negative phase shifts $^1\delta_0(E)$,$^3\delta_0(E)$ belonging to other channels, and affect the bound $1s$ nucleon, i.e., the medium modification of the triton. They lead to the negative values of the virial coefficient given in Ref. [50] but will not be discussed here.

In contrast to ^{5}He, the effective excitation energies for ^{4}H are large and the values for the scattering phase shifts in the corresponding channels are small. They are strongly influenced by the introduction of the quasiparticle picture [the sin term in Eq. (44)] and the Pauli blocking effects, as seen by the increase of the the effective excitation energies with density and temperature.

V. ILLUSTRATIVE CALCULATION OF THE COMPOSITION OF ASYMMETRIC NUCLEAR MATTER

A. Virial, excited states and continuum correlations

Having the partial densities $n^{\mathrm{part}}_c(T,\mu_n,\mu_p)$ of the component c, the composition of nuclear matter is described by the mass fractions $X_c = A_c n^{\mathrm{part}}_c/n_B$ with $\sum_c X_c = 1$. This composition is of interest for different applications such as HIC or astrophysical simulations. For instance, the role of the lightest p nuclei in the composition and the EoS has been discussed recently [17]. Such correlations determine the neutrino opacity, but the inclusion of the lightest p nuclei to evaluate the EoS and the composition demands special attention.

As an illustrative example, the composition of nuclear matter is evaluated for parameter values $T = 10$ MeV, $Y_p = 0.1$, as function of the mass density ρ ($n_B = 0.0597015 \times 10^{-14}\rho$ cm^3/g/fm^3, saturation baryon number density $n_{\mathrm{sat}} = 0.15$ fm^{-3}, mass density $\rho_{\mathrm{sat}} = 10^{14.4}$ g cm^{-3}). The subsaturation density region $\log_{10}\rho$ [g/cm^3] = 11–14 is considered. Asymmetric matter with a small value of Y_p is of interest in stellar processes. As shown in Ref. [17], Fig. 5, higher clusters (metals, $Z > 2$) are not relevant in this region. Using standard approaches such as the NSE and the excluded volume model [18], near the saturation density a large mass fraction of neutron-rich unstable H and He isotopes is predicted.

In order to discuss the account of in-medium corrections, different approximations are compared starting from a simple NSE approach. As a result, it will be shown that the contribution of unstable, neutron-rich isotopes to the composition is strongly reduced near the saturation density if in-medium effects are taken into account.

The simple NSE model neglects all interaction beyond reactive collisions to establish the chemical equilibrium of the components. The large asymmetry $Y_p = 0.1$ prefers the formation of neutron-rich clusters. Considering only the nearly stable elements n, p, d, t, h, α, at high densities ($\log_{10}[\rho] > 13$), t becomes dominant and almost all protons are bound to t. The inclusion of the subsequent neutron-rich, unbound isotopes ^{4}H and ^{5}He with known binding energies [22] into the NSE leads to changes in the high-density region (see Fig. 6, dashed lines).

Instead of t, ^{4}H becomes dominant. In the density region $\log_{10}[\rho] > 13$, almost each proton is bound to this neutron-rich isotope. Similarly, ^{5}He becomes larger than the α mass fraction. In the NSE calculation, known excited states of the nuclei according to the tables [22] are taken into account. In particular, there exists a low-lying level of ^{4}H at 0.31 MeV excitation energy and $J = 1$.

One can continue to include even further known isotopes such as ^{5}H, ^{6}H, ^{7}H, ^{6}He, ^{7}He, ^{8}He, etc., with known binding energies and degeneracy found in the tables [22]. As shown in Ref. [17], Fig. 5, for the NSE model as well as for the excluded volume model, according to the mass action law the effect of the dominance of neutron-rich isotopes becomes even

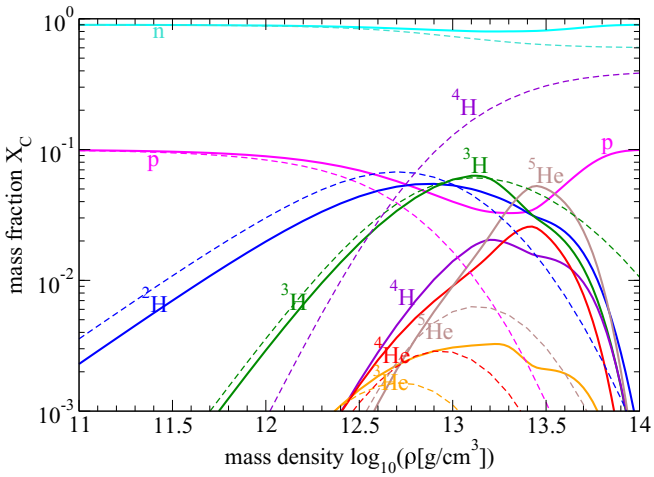

FIG. 6. Composition of nuclear matter, $T = 10$ MeV, $Y_p = 0.1$, as function of the mass density including ^{4}H and ^{5}He. The NSE without excited states (dashed) is compared to this quantum statistical in-medium approach (full lines).

more visible, and matter near saturation density $\log_{10}[\rho] \approx 14$ appears as a mixture of free neutrons, ^{7}H, ^{8}He, and other unbound nuclei. It is evident that a model of noninteracting, unbound nuclei is not adequate to describe matter near the saturation density. It will be shown in the subsequent sections that the mass fractions of all these weakly bound nuclei are strongly suppressed near the saturation density if in-medium corrections are taken into account.

One can also add to the NSE further known nuclei with $Z > 2$. However, the mass fractions are very small (below 10^{-3}) at the parameter values for T, Y_p considered here.

Surprisingly, also in the low-density limit the NSE model fails to describe correctly the composition of the system because, like excited states, also scattering states have to be included. Unbound states are not stable and appear as a resonance in the continuum of scattering states. Above I referred to ^{8}Be which appears in the two-α continuum. Instead of considering a resonance gas, one has to treat the continuum of scattering states consistently.

A systematic treatment not only of the contribution of excited states, but of the whole continuum of scattering states is given by the Beth-Uhlenbeck formula; see Eq. (27) for the case $A = 2$. In the channel $A = 2, Z = 1, J = 0, 1$ the contribution of the scattering states has been parametrized over the temperature range $1 \leqslant T \leqslant 20$ MeV; see Ref. [51]. The second virial coefficient $b_{pn}(T)$ contains the contribution of the deuteron bound state but is reduced owing to the negative contributions of the continuum, in particular at increasing T. Another parametrization is given in Ref. [27]. Virial coefficients for other channels such as ^{4}Li and ^{4}H are found in Ref. [50].

I introduce the virial terms for d, ^{4}H, and ^{5}He as described in Sec. IV. There is a significant reduction of d and a large reduction of ^{4}H. The reason is the small binding energy so that most of the partial density is determined by the integral over the continuum, in particular at increasing T. Because the phase shifts for $t - n$ scattering are small, a strong reduction is obtained from the virial coefficient. A reduction is also observed for ^{5}He, but the $\alpha - n$ phase shifts are rather large so that only a minor reduction results. For a more detailed discussion of the common treatment of bound-state contribution and scattering states, see also Refs. [15,27].

B. Contribution of unbound nuclei ^{4}H and ^{5}He

To investigate the contribution of the unbound nuclei ^{4}H and ^{5}He to the composition of nuclear matter ($T = 10$ MeV, $Y_p = 0.1$), I use the expressions for the corresponding channels given in Sec. IV, Eqs. (37) and (38) for the ^{5}He channel and Eqs. (49) and (50) for the two ^{4}H channels. As function of density, the composition is shown in Fig. 6 which is obtained within these quantum statistical calculations. An important feature of the account of in-medium effects, in particular Pauli blocking, is the suppression of the cluster mass fractions at near-saturation densities. The mass fractions of n, p increase to the values 0.9 and 0.1, respectively. This is already seen if the quantum statistical treatment of only the light $1s$ nuclei d, t, h, α is compared to the NSO approach [26].

Considering the unbound nuclei ^{4}H and ^{5}He, the position of the edge of continuum should be correctly taken into account. With $C^{(0)}_{^4\mathrm{H}}(T)$ being the phase shift integral (50) in the zero-density limit, omitting the quasiparticle shift, one has the virial form [I put ^{4}H and ^{4}H* together; see Eq. (49)]

$$n^{(0)}_{^4\mathrm{H}} = \frac{(5+3)\times 8}{\Lambda^3} e^{(-E_t+3\mu_n+\mu_p)/T} C^{(0)}_{^4\mathrm{H}}(T)) = \frac{32}{3^{3/2}} n^{(0)}_t e^{\mu_n/T} C^{(0)}_{^4\mathrm{H}}(T), \tag{51}$$

$$n^{(0)}_{^5\mathrm{He}} = \frac{4\times 5^{3/2}}{\Lambda^3} e^{(-E_\alpha+3\mu_n+2\mu_p)/T} C^{(0)}_{^5\mathrm{He}}(T) = \frac{5^{3/2}}{2} n^{(0)}_\alpha e^{\mu_n/T} C^{(0)}_{^5\mathrm{He}}(T). \tag{52}$$

Within the quantum statistical approach, the mass fractions of the corresponding channels are calculated according Eqs. (49) and (40). The in-medium effects are incorporated as quasiparticle shift of t and α [15] so that the in-medium densities n_t, n_α appear, the neutron chemical potential is shifted (see Appendix D) and the in-medium expression $C(T)$, Eq. (50), is taken.

The contribution of the unbound nuclei ^{4}H and ^{5}He is reduced at high densities so that the Mott effect becomes visible. Near the saturation density, the mass fraction of bound clusters are decreasing so that X_n, X_p approach the free quasiparticle limits 0.9, 0.1, respectively. The reduction of weakly bound states originates from the contribution of scattering states as known from the deuteron channel. In addition, the introduction of the quasiparticle description leads to a further reduction owing to the sin term (30), since part of the scattering phase shift (Born approximation) is already taken into account by the self-energy shift of the single-nucleon states. Pauli blocking in dense matter reduces further the contribution of the unbound nuclei. As consequence, one can conclude that the NSE with additional account of these unstable nuclei

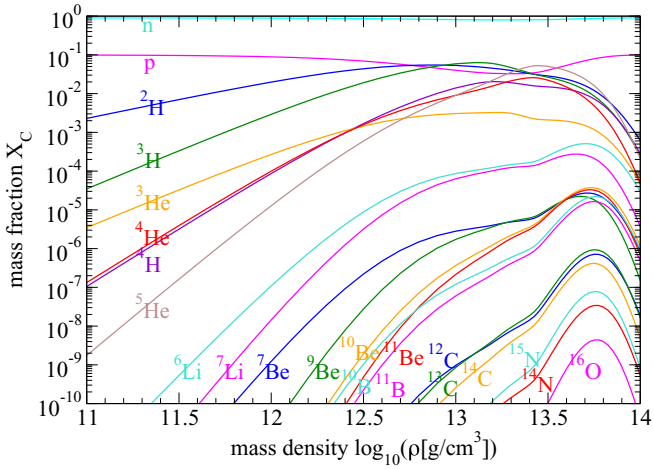

FIG. 7. Composition of nuclear matter, $T = 10$ MeV, $Y_p = 0.1$, as function of the mass density. Continuum edge with self-energy shift according to DD2-RMF at $P = 0$, light elements ($A \leqslant 4$) according to Ref. [15], Pauli blocking in scattering phase shifts by interpolation formulas (42) and (45), and Pauli blocking of light p-shell nuclei according to Eq. (21).

largely overestimates their contribution near the saturation density, as seen in Fig. 6.

C. Light p-shell nuclei in the EoS

Medium effects have a significant influence on the abundances of exotic, light p-shell clusters in dense matter, in particular calculating the composition in thermodynamic equilibrium, Eq. (1). Within the quantum statistical approach, the partial densities of the light p-shell nuclei are calculated with the in-medium energies

$$E_{A,Z,J,\nu}(\mathbf{P};T,\mu_n,\mu_p) = E^{(0)}_{A,Z,J} + \frac{\hbar^2 P^2}{2Am} + \Delta E^{\mathrm{Pauli}}_{A,Z}(\mathbf{P};T,\mu_n,\mu_p) + \Delta E^{\mathrm{SE}}_{A,Z}(\mathbf{P};T,\mu_n,\mu_p). \quad (53)$$

For the Pauli blocking term $\Delta E^{\mathrm{Pauli}}_{A,Z}(P;T,n_B,Y_p)$ I use the interpolation formula (21) as described in Sec. III D. The self-energy term $\Delta E^{\mathrm{SE}}_{A,Z}(\mathbf{P};T,\mu_n,\mu_p)$ is taken as the sum over the self-energy shifts $\Delta E^{\mathrm{SE,RMF}}_{\tau}(T=0,n_B,Y_p)$ of the constituting nucleons, taken here in the DD2-RMF approximation [15,20]; see also Ref. [15]. Because the self-energy shift is present in the bound states as well as the scattering states, it is of minor relevance for the Mott effect. As discussed in Appendix D, a reduction is expected for heavy nuclei so that I take the self-energy shift with a factor 0.5. Up to the Mott density, such additional effects are not essential. Above the Mott density, a further reduction of the contribution of clustered, light p-shell nuclei is expected because one has to treat, instead of bound states, scattering states in the continuum as already presented in the previous Sec. V B.

As an example, calculations are shown in Fig. 7 for the conditions given above, i.e., $T = 10$ MeV and $Y_p = 0.1$ for mass densities $10^{11} \ldots 10^{14}$ g/cm^3. Only the ground states of the nuclei with $A \leqslant 16$ are considered. If comparing the quantum statistical approach to the ordinary NSE, below 10^{12} g/cm^3 both approaches agree quite well; medium effects such as self-energy shifts and Pauli blocking are small. There are deviations because of the virial coefficient containing the continuum contributions, in particular for weakly bound nuclei such as d. The reduction of the abundance of deuterons at high temperatures has been discussed elsewhere [15].

Already at densities of 10^{13} g/cm^3, the mass fraction of clustered, light p-shell nuclei has a maximum and start to be blocked out. This happens before the neutron-rich isotopes like ^{10}Be and ^{11}Be become preferred Be isotopes in the strongly asymmetric matter. One sees that for the entire density region at T, Y_p given above the mass fraction of nuclei with $Z > 2$ are below 10^{-3} so that only a marginal change of the mass fractions of light nuclei ($A \leqslant 4$) is seen in comparison to Fig. 6.

I focused on the Pauli blocking effect as the main ingredient to determine the composition of nuclear matter near the saturation density. For a more detailed investigation, one should also consider other effects, in particular self-energy effects; see Appendix D. As discussed there, the single-nucleon self-energy shift should be reduced for heavier nuclei, and by describing the **p** dependence in effective mass approximation, additional changes of the composition at high densities are expected. For densities higher than the Mott density, i.e., $n_B > 0.03$ fm^{-3}, the mass fraction of clustered, light p-shell nuclei is further reduced because one has only continuum contributions which become small for high densities; cf. Fig. 5. Correlations in the medium will further influence the in-medium modifications as discussed in Ref. [15]. One can expect that the composition in the subsaturation region $\rho > 10^{13.5}$ g/cm^3 is in general correctly described, in particular the transition to a Fermi liquid of quasiparticles, but the detailed description of correlations as well as of the stability against phase transitions remains open for future work.

VI. CONCLUSIONS

Just as with the light nuclei with mass number $A \leqslant 4$, the clustered, light p-shell nuclei ($4 \leqslant A \leqslant 16$) are strongly modified in warm dense matter. Compared to the NSE, Pauli blocking leads to a reduction of the cluster abundances in nuclear matter and the dissolution of bound states at increasing densities. The extension of the simple NSE to unstable nuclei like ^{4}H and ^{5}He is problematic. The systematic treatment of continuum correlations using the generalized Beth-Uhlenbeck formulas gives a reduction of the mass fraction at increasing temperatures and densities. The dominant appearance of neutron-rich unstable isotopes in asymmetric matter near the saturation density, as discussed, e.g., in Ref. [17] using improved versions of the NSE, is not supported.

For fixed temperature and increasing density, correlations, in particular in bound states, are formed in low-density nuclear matter according to the mass action law. They are dissolved mainly owing to Pauli blocking near the saturation density (Mott effect), and a single-nucleon quasiparticle approach to

nuclear matter becomes applicable. Interpolation formulas are given to describe the medium modifications of clusters and correlations in dense nuclear matter in the temperature region $1 \leqslant T \leqslant 20$ [MeV] and subsaturation densities. Calculations of the composition of nuclear matter at $T = 10$ MeV and $Y_p = 0.1$ show, in addition to the light nuclei d, t, h, α, a significant contribution of the neutron-rich clusters ^{4}H and ^{5}He in the density region around $n_{\rm sat}/10$, but at baryon number densities exceeding 0.03 fm^{-3} these correlations are reduced by Pauli suppression.

Unbound nuclei like ^{4}H and ^{5}He are treated as correlations in the continuum. Using a generalized Beth-Uhlenbeck approach which is able to implement in-medium effects, the measured scattering phase shifts in the respective reaction channels have been used to give an estimate of the medium dependence of the phase shifts and to evaluate the partial densities of these components. For the bound $1p$ nuclei with mass number $6 \leqslant A \leqslant 16$, the intrinsic nucleon wave function of the A-nucleon cluster is an essential ingredient to evaluate the in-medium shift of the binding energy because of Pauli blocking. Whereas for $10 \leqslant A \leqslant 16$ a shell model is applicable, the clustered nuclei with $6 \leqslant A \leqslant 9$ show a significant subcluster structure which has to be taken into account to calculate the Pauli blocking shift. Simple fit formulas are given for the bound-state energy shifts which can be used to evaluate the composition and related properties of warm and dense matter.

The quantum statistical approach is based on fundamental concepts such as the spectral function and the self-energy. Systematic improvements of this approach are possible considering further many-particle effects. In particular, at densities above 0.03 fm^{-3}, a detailed description of the self-energy as function of momentum and energy as well as correlations in the medium may be a subject of future work to improve the description of correlations in nuclear matter near the saturation density. Semiempirical approaches such as the concept of excluded volume [18] or the generalized RMF [19,20], which are used presently to account for in-medium effects in the nuclear matter EoS, can profit to get inputs from a more systematic many-particle approach.

Astrophysical applications of the nuclear matter EoS demand the treatment of correlations in dense matter; see, e.g., Refs. [12,13,19,51]. For instance, the neutrino opacity of stellar matter is an important ingredient to describe supernova explosions. The composition of nuclear matter and the formation of correlations determine the neutrino transport in hot and dense matter. The large mass fractions of neutron-rich, unstable isotopes like ^{4}H in stellar matter with low Y_p, which are predicted by NSE and related approaches [17], overestimate these correlations and are not appropriate for calculations of supernova and merger dynamics in the high-density region.

The understanding of few-body correlations in dense matter, in particular bound-state formation, is an important ingredient to describe heavy-ion collisions. Light p-shell nuclei ($4 \leqslant A \leqslant 16$) are observed from HIC experiments; see Ref. [5]. To explain the measured yields, different models can be used such as freeze-out of a fireball, coalescence models, or transport models like AMD or QMD simulations. Compared to the simple NSE approximation for the freeze-out approach, one finds a strong suppression of these yields at increasing densities because of Pauli blocking. Also, for other approaches such as transport models [11], in-medium effects should be taken into account to explain cluster formation in HIC.

The present work may be considered as a first step of a quantum statistical treatment of light $1p$-shell clusters in nuclear matter. To describe the properties of hot and dense nuclear matter, in addition to improvements of the approximations performed here, one has also to extend the treatment of light clusters to heavier nuclei; see Refs. [16,54]. Light clusters, pasta phases, and phase transitions have to be considered in core-collapse supernova matter [55] and mergers. The investigation of few-nucleon correlations in dense matter is a basic prerequisite to understand matter under extreme conditions also in nonequilibrium processes such as heavy-ion collisions.

APPENDIX A: SOLUTION OF THE IN-MEDIUM WAVE EQUATION FOR ^{6}Li

The wave function of ^{6}Li is taken as Gaussian,

$$\psi^{\rm Gauss}_{^6{\rm Li}}(p_1,\ldots,p_6) = \frac{1}{\mathcal{N}_6} e^{-(p_1^2+p_2^2+p_3^2+p_4^2+\beta_6 p_5^2+\beta_6 p_6^2)/B_6^2} p_{5,z} p_{6,z} \delta_{\mathbf{p}_1+\cdots+\mathbf{p}_6,0}\,. \tag{A1}$$

$\mathcal{N}_6$ denotes the normalization factor. I adapt a Gaussian separable interaction

$$V_{^6{\rm Li}}(12,1'2') = \lambda_6\, e^{-\frac{(\mathbf{p}_2-\mathbf{p}_1)^2}{4\gamma_6^2}} e^{-\frac{(\mathbf{p}'_2-\mathbf{p}'_1)^2}{4\gamma_6^2}} \delta_{\mathbf{p}_1+\mathbf{p}_2,\mathbf{p}'_1+\mathbf{p}'_2}. \tag{A2}$$

The rms radius follows as (14)

$$\mathrm{rms}_{^6{\rm Li}} = \left[\frac{\beta_6}{6B_6^2}\frac{21+160/\beta_6+382/\beta_6^2+688/\beta_6^3+288/\beta_6^4}{(1+2/\beta_6)\left(3+8/\beta_6+16/\beta_6^2\right)}\right]^{1/2}. \tag{A3}$$

The intrinsic energy of the ^{6}Li nucleus $E^{(0)}_{^6\mathrm{Li}} = \mathrm{KE}_{^6\mathrm{Li}} + \mathrm{PE}_{^6\mathrm{Li}}$ contains the kinetic and potential energy. For the kinetic energy, one finds

$$\mathrm{KE}_{^6\mathrm{Li}} = \frac{\hbar^2}{2m}\frac{B_6^2}{4\beta_6}\frac{21+160\beta_6+382\beta_6^2+688\beta_6^3+288\beta_6^4}{(1+2\beta_6)\left(3+8\beta_6+16\beta_6^2\right)}. \tag{A4}$$

The potential energy is

$$\mathrm{PE}_{^6\mathrm{Li}} = \lambda_6\left(6V_{12}^x V_{12}^y V_{12}^z + 8V_{15}^x V_{15}^y V_{15}^z + V_{56}^x V_{56}^y V_{56}^z\right) \tag{A5}$$

with

$$V_{12}^x = V_{12}^y = V_{12}^z = \frac{B_6\gamma_6^2}{\pi^{1/2}\left(B_6^2+4\gamma_6^2\right)}, \tag{A6}$$

$$V_{15}^x = V_{15}^y = \frac{2B_6\gamma_6^2(1+2\beta_6)^{1/2}\beta_6^{1/2}}{\pi^{1/2}\left(B_6^2+\gamma_6^2+\beta_6\gamma_6^2\right)^{1/2}\left(B_6^2+8B_6^2\beta_6+3B_6^2\beta_6^2+8\beta_6\gamma_6^2+16\beta_6^2\gamma_6^2\right)^{1/2}}, \tag{A7}$$

V_{15}^z is a lenghtly expression not given here, and

$$V_{56}^x = V_{56}^y = \frac{B_6\gamma_6^2\beta_6^{1/2}}{\pi^{1/2}\left(B_6^2+2\beta_6\gamma_6^2\right)},$$

$$V_{56}^z = \frac{4B_6\gamma^2\beta_6^{5/2}\left(3B_6^4-4B_6^2\beta_6^2+4B_6^2\beta_6\gamma_6^2+4\gamma_6^4+8\beta_6\gamma_6^4+12\beta_6^2\gamma_6^4\right)}{\pi^{1/2}\left(3+8\beta_6+16\beta_6^2\right)\left(B_6^2+2\beta_6\gamma_6^2\right)^3}. \tag{A8}$$

Within a variational approach, the optimum values for B_6, β_6 are obtained from the minimum of the intrinsic energy of the cluster. The parameters λ_6, γ_6 are determined to reproduce the empirical values of the binding energy and the rms radius of ^{6}Li; see Table I. With $\lambda_6 = -964.5$ MeV fm^3 and $\gamma_6 = 1.16$, one finds the optimum values for $B_6 = 1.0626\,\mathrm{fm}^{-1}$ and $\beta_6 = 3.6174$ so that $B_p = 0.5587\,\mathrm{fm}^{-1}$. This result confirms the assumption that B_s changes smoothly (see Table I), whereas β is rather large for ^{6}Li, and the result for B_p agrees reasonably well with the estimated value shown in Table II. Note that the ansatz for the wave function does not include deuteron-like clustering. Deuteron-like correlations are weak, as shown by the low binding energy of d. A calculation including clustering is possible within the THSR ansatz.

The potential energy is modified by the Pauli blocking effect. The evaluation of the shifts $\Delta E^{\mathrm{Pauli,G}}_{^6\mathrm{Li}}(T) = n_B\,\delta E^{\mathrm{Pauli,G}}_{^6\mathrm{Li}}(T)$ according Eq. (5) gives the values shown in Table V for different T. The value at $T = 5$ MeV is also seen in Fig. 3. It is higher than the shell-model value. The large value of β supports the extended character of the $1p$ orbits leading to low densities that favor the formation of clusters.

APPENDIX B: SEPARABLE POTENTIAL MODEL AND ^{5}He AND ^{4}H CONTINUUM CORRELATIONS

The solution of the in-medium wave equation to determine the medium corrections of the scattering phase shifts is convenient for nonlocal, separable potentials. According to Ref. [31], any potential can be represented as a sum of separable potentials. In nuclear physics, separable potentials are introduced, e.g., in Refs. [29,30].

To reproduce the $\delta_{\mathrm{P}_{3/2}}(E)$ of the $\alpha - n$ scattering, I use for the $l = 1$ state

$$V(p,p') = -\frac{\lambda}{\Omega_0}\frac{p}{(p^2/\gamma^2+1)^2}\frac{p'}{(p'^2/\gamma^2+1)^2}. \tag{B1}$$

With

$$I(E) = \frac{\lambda}{2\pi^2}\int_0^\infty dp\,\frac{p^2}{E-\hbar^2p^2/(2m)}\frac{p^2}{(p^2/\gamma^2+1)^4}, \tag{B2}$$

TABLE V. Pauli-blocking shifts $\Delta E^{\mathrm{Pauli,G}}_{^6\mathrm{Li}}(T, n_B) \approx n_B\,\delta E^{\mathrm{Pauli,G}}_{^6\mathrm{Li}}(T)$ for ^{6}Li.

T [MeV]	$\delta E^{\mathrm{Pauli,G}}_{^6\mathrm{Li}}(T)$ [MeV fm^3]
1	3489.7
2	3574.4
3	3457.6
4	3268.9
5	3060.9
6	2855.5
7	2661.7
8	2482.8
9	2319.2
10	2170.4
12	1912.3
14	1698.6
16	1520.4
18	1370.4
20	1243.1

TABLE VI. Second virial coefficient (39) and effective energies $E_{\alpha n}^{\rm eff}(T)$ [MeV] according Eqs. (41) and (42). A separable potential (B1) was used with $\lambda = 670$ MeV fm^3, $\gamma = 1.791$ fm^{-1}, and $T = 2, 4, \ldots, 18, 20$ MeV.

n_n [fm^{-3}]	$E_{\alpha n}^{\rm eff}(2)$	$E_{\alpha n}^{\rm eff}(4)$	$E_{\alpha n}^{\rm eff}(6)$	$E_{\alpha n}^{\rm eff}(8)$	$E_{\alpha n}^{\rm eff}(10)$	$E_{\alpha n}^{\rm eff}(12)$	$E_{\alpha n}^{\rm eff}(14)$	$E_{\alpha n}^{\rm eff}(16)$	$E_{\alpha n}^{\rm eff}(18)$	$E^{\rm eff}(20)$
0.0001	1.525	2.279	3.317	4.639	6.236	8.091	10.185	12.499	15.017	17.723
0.001	1.699	2.481	3.533	4.867	6.474	8.339	10.441	12.764	15.29	18.003
0.01	4.113	4.795	5.931	7.372	9. 084	11.047	13.241	15.647	18.246	21.025
0.02	7.196	7.677	8.859	10.42	12.27	14.366	16.681	19.192	21.882	24.738
0.03	10.3	10.665	11.904	13.603	15.614	17.871	20.33	22.967	25.764	28.708
0.04	13.344	13.669	14.997	16.86	19.061	21.503	24.13	26.912	29.831	32.875
0.05	16.3	16.653	18.112	20.173	22.595	25.247	28.062	31.003	34.054	37.205
0.06	19.167	19.606	21.251	23.556	26.229	29.113	32.129	35.238	38.427	41.689
0.07	21.95	22.547	24.45	27.048	30.001	33.131	36.353	39.632	42.957	46.327
0.08	24.668	25.533	27.787	30.727	33.975	37.35	40.77	44.208	47.659	51.129
0.09	27.389	28.71	31.414	34.716	38.245	41.838	45.429	49.001	52.557	56.109
0.1	30.426	32.45	35.613	39.207	42.938	46.68	50.386	54.049	57.678	61.285
$E_{\alpha n,0}(T)$	1.4157	2.2051	3.2677	4.5979	6.1899	8.033	10.113	12.413	14.918	17.613
$E_{\alpha n,1}(T)$	297.12	271.81	270.21	277.68	288.87	301.18	313.25	324.39	334.35	343.04
$E_{\alpha n,2}(T)$	−68.449	281.09	494.93	649.07	759.83	836.47	887.17	918.99	937.19	945.68

one has

$$I(E) = \frac{\lambda}{\pi} \frac{\gamma^5[-8E^3 - 36E^2\gamma^2\hbar^2/m + 32\sqrt{2}(-E\hbar^2/m)^{3/2}\gamma^3 + 18E(\hbar^2/m)^2\gamma^4 + \gamma^6(\hbar^2/m)^3]}{32(2E + \gamma^2\hbar^2/m)^4}. \tag{B3}$$

Bound states appear at $I(E) = -1$. The scattering phase shifts follow from

$$\delta_1(E) = -\arctan\left(\frac{{\rm Im}I(E)}{1 + {\rm Re}I(E)}\right). \tag{B4}$$

The empirical phase shifts of ^{5}He are well reproduced with the parameter values $\lambda = 670$ MeV fm^3, $\gamma = 1.791$ fm^{-1}; see Sec. IV B. Parameter values for ^{4}H are given in Sec. IV D.

To include Pauli blocking effects, one has to consider in Eqs. (B2) and (B4)

$$I(E; T, \mu_n) = \frac{\lambda}{2\pi^2} \int_0^\infty dp \, \frac{p^2}{E - \hbar^2 p^2/(2m)} \frac{p^2}{(p^2/\gamma^2 + 1)^4} [1 - f_n(p; T, \mu_n)]\,. \tag{B5}$$

The neutron orbital is only blocked by the neutron background with density n_n. I assume an ideal fermion distribution with the chemical potential $\mu_n(T, n_n)$ according to

$$n_n = \frac{1}{\pi^2} \int_0^\infty dp \frac{p^2}{e^{(\hbar^2 p^2/2m - \mu_n)/T} + 1}. \tag{B6}$$

The real part of $I(E; T, n_n)$ is given by the principal value integral; the imaginary part is

$${\rm Im}I(E; T, \mu_n) = \frac{\lambda}{2\pi} \frac{m}{\hbar^2} \left(\frac{2mE}{\hbar^2}\right)^{3/2} \frac{1}{(2Em/(\hbar^2\gamma^2) + 1)^4} \left[1 - \frac{1}{e^{E/T - \mu_n/T} + 1}\right]. \tag{B7}$$

Results for the virial coefficients calculated with in-medium scattering phase shifts are given in Tables VI and VII, together with the corresponding effective energies which are used for the interpolations (43) and (46).

APPENDIX C: SHIFTS AND MOTT DENSITIES FOR SELECTED TEMPERATURES

Within the shell model, the Pauli blocking shift is given by the contributions of occupied $1s$ and $1p$ orbitals according

TABLE VII. $C^{\rm BU}_{^4{\rm H}}(T)$ and effective energies $E^{\rm eff}_{tn}(T)$. A separable potential (B1) was used with $\lambda = 1144.9$ MeV fm^3, $\gamma = 1.326$ fm^{-1}, and $T = 1, 2, 3, 5, 10, 20$ MeV.

n_n [fm^{-3}]	$C^{\rm BU}(1)$	$E^{\rm eff}(1)$	$C^{\rm BU}(2)$	$E^{\rm eff}(2)$	$C^{\rm BU}(3)$	$E^{\rm eff}(3)$	$C^{\rm BU}(5)$	$E^{\rm eff}(5)$	$C^{\rm BU}(10)$	$E^{\rm eff}(10)$	$C^{\rm gBU}(20)$	$E^{\rm eff}(20)$
0.0001	0.008651	4.7502	0.03475	6.7189	0.05832	8.5249	0.08764	12.183	0.1066	22.387	0.094462	47.191
0.001	0.006673	5.0097	0.029987	7.0139	0.05206	8.8655	0.080605	12.591	0.1014	22.882	0.091884	47.744
0.01	0.00008886	9.3283	0.0041078	10.989	0.01361	12.89	0.033803	16.936	0.06141	27.901	0.06955	53.313
0.02	6.236E-7	14.288	0.00036852	15.812	0.002727	17.713	0.012388	21.955	0.0349	33.534	0.050911	59.554
0.03	6.357E-9	18.874	0.00003619	20.453	0.000564	22.439	0.004588	26.921	0.01993	39.155	0.03721	65.826
$E_{\alpha n,0}(T)$		4.6196		6.5808		8.4052		12.095		22.319		47.114
$E_{\alpha n,1}(T)$		477.15		459.68		464.96		492.79		560.79		622.89

Eq. (18). For symmetric matter, one has

$$\begin{aligned}\Delta E^{\rm Pauli}_{A,Z}(P=0;T,\mu_n,\mu_p) &\approx n_B\left[4\,\delta E^{\rm Pauli}_{AZ,s}(T)+(A-4)\,\delta E^{\rm Pauli}_{AZ,p}(T)\right]\\ &= n_B\,\delta E^{\rm Pauli}_{A,Z}(P=0;T). \end{aligned} \tag{C1}$$

For the light p-shell nuclei, both contributions are given in Table VIII at selected temperatures $T = 5, 10, 15$, and 20 MeV. The Mott density $n^{\rm Mott}_{A,Z}(T) = B_{A,Z}/\delta E^{\rm Pauli}_{A,Z}(P=0;T)$ describes the baryon number density where at $P = 0$ the bound state merges with the continuum and disappears. Values for $n^{\rm Mott}_{A,Z}(T)$ are also given in Table VIII. Note that above the Mott density A-nucleon correlations survive because bound states with large c.m. momentum **P** can exist (the Pauli blocking becomes smaller; see Fig. 1). In addition, A-nucleon continuum correlations remain.

APPENDIX D: SINGLE-NUCLEON SELF-ENERGY SHIFTS

Single-particle excitations in nuclear systems are described by the single-nucleon spectral function $A_\tau(\mathbf{p},\omega)$, which is determined by the dynamical self-energy $\Sigma_\tau(\mathbf{p},\omega)$. In the quasiparticle approach, the spectral function is approximated by a δ-like single-particle contribution and a background. The quasiparticle dispersion relation $E^{\rm qu}_\tau(\mathbf{p}) = \hbar^2p^2/(2m_\tau) + \Delta E^{\rm SE}_\tau(\mathbf{p})$ contains the self-energy shift $\Delta E^{\rm SE}_\tau(\mathbf{p}) = \Sigma_\tau[\mathbf{p},\omega = E^{\rm qu}_\tau(\mathbf{p})]$.

The concept of quasiparticle excitation proved to be successful at low densities as well as high densities (Fermi liquid). A criterion is that further correlations which determine the background of the spectral function are not significant. The quasiparticle shift can be related to empirical data; I use here the DD2-RMF approximation [25]. For instance, at $T = 0$ the quasiparticle shift in the low-density limit amounts to (units MeV, fm)

$$\begin{aligned}\Delta E^{\rm SE,RMF}_\tau&(T=0,n_B,Y_p)\\ &\approx [-1058.4+490.15\,{\rm sgn}_\tau(1-2Y_p)\\ &\quad -1.659(1-2Y_p)^2-0.00761\,{\rm sgn}_\tau(1-2Y_p)^3\\ &\quad -0.2668(1-2Y_p)^4]n_B+\mathcal{O}(n_B^2),\end{aligned} \tag{D1}$$

with ${\rm sgn}_\tau = 1$ for $\tau = n$ and ${\rm sgn}_\tau = -1$ for $\tau = p$.

The microscopic approach to the self-energy can be performed using the method of Green's functions and diagram representations, but needs also an expression for the interaction potential. In lowest order of interaction, one obtains the

TABLE VIII. Temperature-dependent shifts $\delta E^{\rm Pauli}_{AZ,s}(T)$ and $\delta E^{\rm Pauli}_{AZ,p}(T)$ of $1s$, $1p$ nuclei, $A' = A - 4$. The corresponding Mott densities $n^{\rm Mott}_{A,Z}(T)$ are also given. Units: MeV, fm.

T	=	5 MeV	5 MeV	5 MeV	10 MeV	10 MeV	10 MeV	15 MeV	15 MeV	15 MeV	20 MeV	20 MeV	20 MeV
A	Z	$4\delta E^{\rm Pauli}_{AZ,s}$	$A'\delta E^{\rm Pauli}_{AZ,p}$	$n^{\rm Mott}_{A,Z}$	$4\delta E^{\rm Pauli}_{AZ,s}$	$A'\delta E^{\rm Pauli}_{AZ,p}$	$n^{\rm Mott}_{A,Z}$	$4\delta E^{\rm Pauli}_{AZ,s}$	$A'\delta E^{\rm Pauli}_{AZ,p}$	$n^{\rm Mott}_{A,Z}$	$4\delta E^{\rm Pauli}_{AZ,s}$	$A'\delta E^{\rm Pauli}_{AZ,p}$	$n^{\rm Mott}_{A,Z}$
4	2	2389.7		0.01184	1691.5		0.01673	1277.3		0.02216	1008.2		0.02807
6	3	2596.8	226.8	0.01133	1777.7	175.5	0.01638	1313.5	132.5	0.02212	1021.1	103.2	0.02846
7	3	2695.5	422.7	0.01258	1821.0	374.4	0.01788	1334.2	304.0	0.02395	1031.2	247.8	0.03068
7	4	2695.5	378.1	0.01223	1821.0	307.8	0.01766	1334.2	238.7	0.02391	1031.2	188.9	0.03082
9	4	2888.5	796.3	0.01578	1908.6	709.1	0.02222	1379.3	577.5	0.02972	1056.1	471.5	0.03807
10	4	2976.8	1240.6	0.01541	1948.2	1236.8	0.02040	1399.7	1076.1	0.02624	1067.5	917.3	0.03275
11	4	3074.9	1453.6	0.01446	1995.1	1401.2	0.019281	1425.9	1194.5	0.02499	1083.6	1004.5	0.03136
10	5	2976.8	1172.5	0.01561	1948.2	1133.7	0.02101	1399.7	968.3	0.02734	1067.4	815.4	0.03439
11	5	3074.9	1520.9	0.01658	1995.1	1500.5	0.02180	1425.9	1297.1	0.02799	1083.6	1100.9	0.03469
12	6	3161.4	1792.7	0.01860	2034.5	1737.1	0.02443	1446.9	1485.5	0.03143	1095.9	1251.7	0.03927
13	6	3257.5	2198.8	0.01779	2081.2	2152.2	0.02294	1473.7	1851.4	0.02921	1113.0	1566.2	0.03624
14	6	3342.0	2537.8	0.01791	2119.8	2456.5	0.02301	1494.6	2099.0	0.02930	1125.7	1767.7	0.03639
14	7	3342.0	2419.4	0.01817	2119.8	2294.1	0.02371	1494.6	1936.4	0.03051	1125.7	1617.6	0.03815
15	7	3437.2	2738.7	0.01870	2165.6	2562.8	0.02442	1520.9	2146.4	0.03149	1142.5	1783.9	0.03946
16	8	3524.6	2945.7	0.01972	2206.9	2678.4	0.02612	1544.3	2206.2	0.03403	1157.3	1813.7	0.04295

Hartree-Fock approximation

$$\Delta E^{\mathrm{SE,HF}}_{\tau_1}(1) = \sum_2 [V(12,12) - V(12,21)] f(2). \quad \text{(D2)}$$

For instance, the Hartree shift of the simple Yukawa potential

$$V^{\mathrm{Yukawa}}(r) = -\lambda \exp[-r/R_\pi]/r \quad \text{(D3)}$$

with $R_\pi = 1.4$ fm reproduces (D1) for symmetric matter ($Y_p = 1/2$) if the parameter value $\lambda = 42.97$ MeV fm is chosen.

There exist more realistic nucleon-nucleon interactions and higher order diagram approximations such as the Brueckner-Hartree-Fock approximation considering ladder sums for the self-energy; see also Ref. [14]. Correlations in the medium may be taken into account, leading to the cluster mean-field approximation [27]. The consideration of higher order diagrams allows to introduce the two-particle distribution function as known from the average potential energy in classical statistics.

For nuclei, the effective interaction with free nucleons can be modeled by an optical potential. A recent version for $A \leqslant 13$ has been given in Ref. [52]. It can be approximated by the folding integral of the Yukawa interaction with the density distribution of nucleons in the core nucleus. I will not present here details of such model calculations.

Whereas the interaction outside the nucleus is reasonably described by a Yukawa-like potential (see also the M3Y potential [53]), slow free nucleons can only hardly enter the nucleus because of the Pauli principle. This is a higher order effect, the core nucleon is part of the cluster which determines the Pauli-forbidden region in the phase space. In higher orders of perturbation theory, one has to include diagrams leading to the pair distribution function $g(r)$, as also seen in the cluster mean-field approximation [15]. The pair distribution function becomes small at the surface of the core nucleus, radius $R_A = (4\pi n_{\mathrm{sat}}/3)^{-1/3} A^{1/3} = 1.17 A^{1/3}$ fm. As a consequence, the mean field given by the average potential is also reduced if short distances between the cluster nucleon and the free environmental nucleon are avoided. This effect should be taken into account if larger nuclei in matter are considered. A more sophisticated evaluation, considering higher order diagrams to describe the antisymmetrization of the outside free nucleon with respect to all nucleons bound in the cluster, may be a topic of future investigations if heavy clusters in matter are considered.

To give an estimate of the reduction of the nucleon pair distribution inside the nucleus, I cut the Hartree term at the surface of the nucleus,

$$\Delta E^{\mathrm{SE,cut}} = 4\pi \int_{R_A}^{\infty} dr\, r^2\, V^{\mathrm{Yukawa}}(r). \quad \text{(D4)}$$

Compared to the value at $R_A = 0$, one has the reduction 0.68 for $A = 6$, and 0.48 for $A = 16$. One concludes that the single-nucleon self-energy shift is reduced by a factor of about $1/2$ in the region $6 \leqslant A \leqslant 16$.

This effect will not change the general feature of the formation and dissolution of clusters when the baryon density rises to the saturation density. It is not of relevance for the composition at low densities but modifies the composition near n_{sat}. Note that further effects are obtained from the effective mass corrections; see Ref. [26]. With the empirical value for the effective mass given there, the binding energy of the cluster is slightly reduced.

[1] P. Ring and P. Schuck, *The Nuclear Many-Body Problem* (Springer, Berlin, 1980).
[2] A. Tohsaki, H. Horiuchi, P. Schuck, and G. Röpke, Phys. Rev. Lett. **87**, 192501 (2001).
[3] A. Tohsaki, H. Horiuchi, P. Schuck, and G. Ropke, Rev. Mod. Phys. **89**, 011002 (2017).
[4] S. Yang, C. Xu, G. Röpke, P. Schuck, Z. Ren, Y. Funaki, H. Horiuchi, A. Tohsaki, T. Yamada, and B. Zhou, Phys. Rev. C **101**, 024316 (2020).
[5] T. A. Armstrong *et al.*, Phys. Rev. C **65**, 014906 (2001).
[6] H. Pais *et al.*, arXiv:1911.10849.
[7] G. Röpke, L. Münchow, and H. Schulz, Nucl. Phys. A **379**, 536 (1982); Phys. Lett. B **110**, 21 (1982).
[8] A. S. Botvina and I. N. Mishustin, Nucl. Phys. A **843**, 98 (2010); N. Buyukcizmeci *et al.*, *ibid.* **907**, 13 (2013).
[9] E. Beth and G. E. Uhlenbeck, Phys. (Amsterdam, Neth.) **4**, 915 (1937).
[10] C. J. Horowitz and A. Schwenk, Nucl. Phys. A **776**, 55 (2006).
[11] J. Xu *et al.*, Phys. Rev. C **93**, 044609 (2016).
[12] T. Fischer *et al.*, Astrophys. J, Suppl. Ser. **194**, 39 (2011).
[13] T. Fischer, M.-R. Wu, B. Wehmeyer, N. Bastian, G. Martínez-Pinedo, and F. Thielemann, Astrophys. J. **894**, 9 (2020).
[14] M. Schmidt, G. Röpke, and H. Schulz, Ann. Phys. (NY) **202**, 57 (1990).
[15] G. Röpke, Phys. Rev. C **92**, 054001 (2015).
[16] G. Röpke, J. Phys.: Conf. Ser. **436**, 012070 (2013).
[17] A. V. Yudin, M. Hempel, S. I. Blinnikov, D. K. Nadyozhin, and I. V. Panov, Monthly Not. Royal Astron. Soc **483**, 5426 (2019).
[18] M. Hempel and J. Schaffner-Bielich, Nucl. Phys. A **837**, 210 (2010).
[19] H. Pais, F. Gulminelli, and C. Providencia, and G. Röpke, Phys. Rev. C **99**, 055806 (2019).
[20] S. Typel, G. Ropke, T. Klahn, D. Blaschke, and H. H. Wolter, Phys. Rev. C **81**, 015803 (2010).
[21] G. Audi *et al.*, Nucl. Phys. A **729**, 337 (2003); M. Wang, G. Audi *et al.*, Chin. Phys. C **41**, 030001 (2017).
[22] NuDat/Chart of Nuclides, http://www.nndc.bnl.gov; https://www-nds.iaea.org/relnsd/vcharthtml/VChartHTML.html.
[23] G. Röpke *et al.*, Nucl. Phys. A **897**, 70 (2013).
[24] M. D. Voskresenskaya and S. Typel, Nucl. Phys. A **887**, 42 (2012).
[25] S. Typel, Phys. Rev. C **71**, 064301 (2005); S. Typel and H. H. Wolter, Nucl. Phys. A **656**, 331 (1999).
[26] G. Röpke, Phys. Rev. C **79**, 014002 (2009).

[27] G. Röpke, Nucl. Phys. A **867**, 66 (2011).
[28] N. Schwierz, I. Wiedenhover, and A. Volya, arXiv:0709.3525.
[29] Y. Yamaguchi, Phys. Rev. **95**, 1628 (1954).
[30] T. R. Mongan, Phys. Rev. **175**, 1260 (1968); **178**, 1597 (1969); **180**, 1514 (1969).
[31] D. J. Ernst, C. M. Shakin, and R. M. Thaler, Phys. Rev. C **8**, 46 (1973); D. J. Ernst, C. M. Shakin, R. M. Thaler, and D. L. Weiss, *ibid.* **8**, 2056 (1973).
[32] M. Asplund, N. Grevesse, A. J. Sauval, and P. Scott, Annu. Rev. Astron. Astrophys. **47**, 481 (2009).
[33] I. Angeli and K. P. Marinova, At. Data Nucl. Data Tables **99**, 69 (2013).
[34] M. Lyu, Z. Ren, B. Zhou, Y. Funaki, H. Horiuchi, G. Röpke, P. Schuck, A. Tohsaki, C. Xu, and T. Yamada, Phys. Rev. C **91**, 014313 (2015).
[35] Q. Zhao *et al.*, Phys. Rev. C **100**, 014306 (2019).
[36] Y. Kanada-En'yo and H. Horiuchi, Prog. Theor. Phys. **142**, 205 (2001).
[37] K. Wildermuth and Y. C. Tang, *A Unified Theory of the Nucleus* (Vieweg, Braunschweig, Germany, 1977).
[38] S. Saito, Prog. Theor. Phys. Suppl. **62**, 11 (1977).
[39] H. Horiuchi, Prog. Theor. Phys. Suppl. **62**, 90 (1977).
[40] H. Horiuchi, K. Ikeda, and K. Kato, Prog. Theor. Phys. Suppl. **192**, 1 (2012).
[41] R. B. Wiringa, S. C. Pieper, J. Carlson, and V. R. Pandharipande, Phys. Rev. C **62**, 014001 (2000).
[42] M. V. Egorov, Nucl. Phys. A **987**, 247 (2019).
[43] K. Huang, *Statistical Mechanics*, 2nd ed. (Wiley, New York, 1987).
[44] B. Hoop and H. H. Barschall, Nucl. Phys. **83**, 65 (1966).
[45] R. A. Arndt and L. D. Roper, Phys. Rev. C **1**, 903 (1970).
[46] J. D. Seagrave, J. C. Hopkins, D. R. Dixon, P. W. Keaton, Jr., E. C. Kerr, A. Niiler, R. H. Sherman, and R. K. Walter, Ann. Phys. (NY) **74**, 250 (1972).
[47] M. LeMere, R. E. Brown, Y. C. Tang, and D. R. Thompson, Phys. Rev. C **12**, 1140 (1975).
[48] P. N. Shen, Y. C. Tang, H. Kanada, and T. Kaneko, Phys. Rev. C **33**, 1214 (1986).
[49] I. Reichstein, D. R. Thompson, and Y. C. Tang, Phys. Rev. C **3**, 2139 (1971).
[50] E. O'Connor, D. Gazit, C. J. Horowitz, A. Schwenk, and N. Barnea, Phys. Rev. C **75**, 055803 (2007).
[51] C. J. Horowitz, G. Shen, E. O'Connor, and C. D. Ott, Phys. Rev. C **86**, 065806 (2012).
[52] S. P. Weppner, J. Phys. G: Nucl. Part. Phys. **45**, 095102 (2018).
[53] G. R. Satchler and W. G. Love, Phys. Rep. **55**, 183 (1979).
[54] F. Gulminelli and A. R. Raduta, Phys. Rev. C **92**, 055803 (2015); A. R. Raduta and F. Gulminelli, *ibid.* **82**, 065801 (2010); H. Pais, F. Gulminelli, C. Providencia, and G. Ropke, *ibid.* **97**, 045805 (2018).
[55] H. Pais, S. Chiacchiera, and C. Providencia, Phys. Rev. C **91**, 055801 (2015).